

# Spatial Bayesian GLM on the cortical surface produces reliable task activations in individuals and groups

Daniel Spencer<sup>\*1</sup>, Yu (Ryan) Yue<sup>2</sup>, David Bolin<sup>3</sup>, Sarah Ryan<sup>4</sup>, and Amanda F. Mejia<sup>1</sup>

<sup>1</sup>Department of Statistics, Indiana University, Myles Brand Hall E104 901 E. 10th Street Bloomington, IN, 47408, USA

<sup>2</sup>Paul H. Chook Department of Information Systems and Statistics, Baruch College, The City University of New York, New York, NY, 10010, USA

<sup>3</sup>CEMSE Division, King Abdullah University of Science and Technology, Thuwal, Makkah Province, 23955-6900, Saudi Arabia

<sup>4</sup>Perelman School of Medicine, University of Pennsylvania, Philadelphia, PA, 19104, USA

April 16, 2022

## Abstract

The general linear model (GLM) is a widely popular and convenient tool for estimating the functional brain response and identifying areas of significant activation during a task or stimulus. However, the classical GLM is based on a massive univariate approach that does not explicitly leverage the similarity of activation patterns among neighboring brain locations. As a result, it tends to produce noisy estimates and be underpowered to detect significant activations, particularly in individual subjects and small groups. A recently proposed alternative, a cortical surface-based spatial Bayesian GLM, leverages spatial dependencies among neighboring cortical vertices to produce smoother and more accurate estimates and areas of functional activation. The spatial Bayesian GLM can be applied to individual and group-level analysis. In this study, we assess the reliability and power of individual and group-average measures of task activation produced via the surface-based spatial Bayesian GLM. We analyze motor task data from 45 subjects in the Human Connectome Project (HCP) and HCP Retest datasets. We also extend the model to multi-session analysis and employ subject-specific cortical surfaces rather than surfaces inflated to a sphere for more accurate distance-based modeling. Results show that the surface-based spatial Bayesian GLM produces highly reliable activations in individual subjects and is powerful enough to detect trait-like functional topologies. Additionally, spatial Bayesian modeling enhances reliability of group-level analysis even in moderately sized samples ( $n = 45$ ). Notably, the power of the spatial Bayesian GLM to detect activations above a scientifically meaningful effect size is nearly invariant to sample size, exhibiting high power even in small samples ( $n = 10$ ). The spatial Bayesian GLM is computationally efficient in individuals and groups and is convenient to implement with the open-source **BayesfMRI** R package.

**Keywords**— task fMRI, Bayesian, general linear model, cortical surface

---

<sup>\*</sup>Corresponding author: Daniel Spencer, danieladamspencer@gmail.com

# 1 Introduction

The functional topology of the human brain has been shown to be highly individualized, thanks to recent studies collecting large amounts of functional magnetic resonance imaging (fMRI) data on individual subjects [Gordon et al., 2020, Laumann et al., 2015, Choe et al., 2015, Braga and Buckner, 2017, Kong et al., 2019, Barch et al., 2013]. Functional boundaries have been shown to be consistent under task and rest conditions [Laumann et al., 2015] and to be predictive of behavior [Kong et al., 2019]. Unfortunately, uncovering individualized functional topology has often relied on collecting vast amounts of data on individual subjects, which is infeasible in many settings due to practical constraints and participant considerations. Some populations of vital research and clinical interest are generally unable to undergo long or frequent scans, including young children, the elderly, or those with developmental disorders or suffering from neurodegenerative disease. Recently, practical Bayesian techniques have been proposed as a way to extract reliable and predictive measures of brain organization in individuals based on much shorter scan duration by leveraging information shared across multiple observations to improve estimation [Bzdok and Yeo, 2017, Kong et al., 2019, Mejia et al., 2020a].

However, most analyses of task fMRI continue to focus on estimating group-level effects using conventional analytical methods, particularly in the absence of large amounts of data on individuals. Group-level analyses are favored in part because individual-level measures of task activation produced using the classical “massive univariate” general linear model (GLM) have been found to be unreliable [Elliott et al., 2020]. In the classical GLM, which is popular due to its simplicity and computational efficiency, a separate linear model is fit at every location of the brain relating observed blood oxygenation level dependent (BOLD) activity to the expected hemodynamic response to a series of tasks or stimuli [Friston et al., 1995]. Task activation amplitude shows strong local spatial dependence, but information shared across locations is not leveraged at this stage except through ad-hoc smoothing [Mikl et al., 2008]. To identify areas of activation due to each task, a  $t$ -test is then performed at each location, which requires correcting for the massive number of multiple comparisons this involves. This correction, combined with failure to fully leverage information shared across brain locations, often results in a lack of power to detect many true activations at the group level for small sample sizes (e.g.,  $n = 20$  to  $30$ ), and even more so in individual subjects [Lindquist and Mejia, 2015, Cremers et al., 2017].

While group-level discoveries using task fMRI have greatly advanced general understanding of brain function and organization, as well as systematic differences related to disease, condition, and normal development and aging, individual-level measures are vital for advancing fMRI-based research to new frontiers. Longitudinal modeling, biomarker discovery, therapeutic clinical trials, translation of research findings into clinical practice, and pre-surgical planning all depend on extracting accurate measures of brain function and organization in individual subjects, often without the luxury of long or multiple sessions of data. Therefore, it is vital to develop more powerful and accurate methods. A promising direction is to incorporate expected patterns of spatial dependence and sparsity in activation amplitude [Zhang et al., 2015] through spatial Bayesian models. Several such models have been proposed for volumetric (typically slice-wise) analysis [Spencer et al., 2020, Zhang et al., 2014, 2015, 2016]. Yet there is growing evidence in favor of surface-based analyses to improve sensitivity, power and reproducibility [Fischl et al., 1999, Anticevic et al., 2008, Tucholka et al., 2012, Glasser et al., 2013, Brodoehl et al., 2020]. Importantly, surface-based analysis avoids spurious activations induced by mixing signals across distinct cortical areas [Glasser et al., 2013, Brodoehl et al., 2020], which can occur in standard volumetric smoothing as well as spatial Bayesian models applied to volumetric data, since they implicitly smooth activations.

Recently, Mejia et al. [2020b] proposed a novel surface-based spatial Bayesian GLM, which combines the benefits of spatial modeling and the advantages of cortical surface analysis. In this framework, activation amplitudes are based on the mean of the posterior distribution for each task, which incorporates spatial dependence and sparsity from the prior, yielding smoother and more focal regions of peak activation. Areas of activation are identified using the joint posterior distribution through an excursions set approach [Bolin and Lindgren, 2015], avoiding the need for multiple comparisons correction and greatly increasing power. Group effects can be estimated through a computationally efficient approach based on combining the results of each subject-level model in a principled way. The Bayesian computation is performed using integrated nested Laplace approximations (INLA) [Rue et al., 2009], which is computationally efficient and does not suffer from the inaccuracies common to variational Bayesian approaches [Sidén et al., 2017], which have been commonly used in volumetric spatial Bayesian analyses.

This approach was validated by Mejia et al. [2020b] through simulation studies and a study of twenty individuals from the Human Connectome Project (HCP) [Barch et al., 2013]. These analyses showed a major improvement to estimation efficiency and power, relative to the classical massive univariate GLM. However, this approach has not yet been fully validated in a larger sample, and how accurately it estimates brain function and organization reflecting individualized functional topology remains to be determined.



In this paper, we extensively validate the surface-based spatial Bayesian GLM framework as an alternative to the classical GLM applied to cortical surface data. We illustrate the gain in power and statistical efficiency of the Bayesian approach for both subject-level and group-level analyses, particularly for shorter scan durations. To assess the ability of the Bayesian approach to extract unique individual-level insights, we examine how reliable the Bayesian estimates and areas of activation.

We also extend the original model proposed by Mejia et al. [2020b] in two important ways. First, in the original model, the spherical surfaces from each subject were used as the spatial domain. Inflation to the sphere, while useful for inter-subject registration, distorts the distances between neighboring vertices up to 3-fold (Appendix **Figure A.1**). This has implications for the smoothing of task activations performed implicitly in the Bayesian model, because the degree of dependence between neighbors is a function of the distance between them. In this work, we use the midthickness surface of each individual subject having been registered to the fsaverage32k template, which was created using the FreeSurfer software platform [Fischl, 2012] and is freely available in the HCP data release [Barch et al., 2013]. This surface geometry respects the individual anatomical features of each individual subject and preserves the geodesic distances between locations along the cortical surface, while aligning vertices across subjects for possible group-level analysis.

Second, the original model was proposed for single-subject, single-run analysis (with group-level analysis possible through a principled post-hoc approach). Here, we generalize the model to multi-run analysis. In this framework, separate run-specific estimates and areas of activation are produced, along with cross-run averages. A major advantage of the multi-run model is that hyperparameters controlling the spatial properties of each task activation field are shared across runs, improving estimation efficiency.

The remainder of this paper is organized as follows. The 2 section will outline the surface-based spatial Bayesian GLM and the classical GLM, and will also include a description of the data, the model estimation procedure, and the reliability metrics. Section 3 will outline the application and results of analyses of the motor task data from the Human Connectome Project [Barch et al., 2013] using the classical and Bayesian GLMs. Section 4 will summarize the findings.

## 2 Methods

### 2.1 Surface-Based Spatial Bayesian GLM

The subject-level surface-based spatial Bayesian (SBSB) GLM proposed by Mejia et al. [2020b] consists of two stages: model estimation and identifying areas of activation. **Figure 1** illustrates both stages in contrast with the classical GLM. Below, we describe each stage briefly, including our novel multi-run extension. The SBSB GLM also allows for computationally efficient group-level estimation, described below. For more details on the mathematical construction and Bayesian computation of the SBSB model, see Mejia et al. [2020b].

#### 2.1.1 Single-subject modeling

**Single-run model.** Let  $N$  be the number of vertices on the cortical surface where BOLD signal is measured, and let  $T$  be the duration of the fMRI timeseries. The classical GLM [Friston et al., 1995] adapted to the cortical surface is based on fitting a separate regression model at each vertex. In each model, the response is the observed BOLD activity, and the predictors are the expected BOLD response due to each of  $K$  tasks or stimuli, which is constructed by convolving the timeseries of stimulus presentation with a haemodynamic response function (HRF). For simplicity, assume that nuisance signals (e.g. head motion parameters, drift) have been regressed from both the response and task predictors, and assume that the data has been prewhitened to remove temporal autocorrelation in the model residuals and to eliminate spatial heterogeneity in the residual variance. Then, the classical GLM at vertex  $v$  can be represented as

$$\mathbf{y}_v = \mathbf{X}_v \boldsymbol{\beta}(v) + \boldsymbol{\epsilon}_v, \quad (1)$$

where  $\mathbf{y}_v \in \mathbb{R}^T$  is the observed BOLD timeseries,  $\mathbf{X}_v \in \mathbb{R}^{T \times K}$  contains the expected response to each of the  $K$  stimuli,  $\boldsymbol{\beta}(v) \in \mathbb{R}^K$  are the coefficient values representing the activation amplitude for each stimulus at a single vertex  $v$ , and  $\boldsymbol{\epsilon}_v \stackrel{\text{ind}}{\sim} \text{Normal}(\mathbf{0}, \sigma^2 \mathbf{I}_T)$  are white-noise residuals. Note that  $\mathbf{X}_v$  may vary across vertices

due to prewhitening, which involves pre-multiplying the original design matrix by a vertex-specific whitening matrix. If no prewhitening is performed, then  $\mathbf{X}_1 = \dots = \mathbf{X}_N$ . While computationally convenient and simple, fitting thousands of separate models is clearly suboptimal, since neighboring vertices are known to exhibit similar patterns of task activation. If these similarities are not explicitly modeled, the estimates of activation will contain high levels of noise due to reduced statistical efficiency.

A spatial Bayesian GLM addresses this by treating the *image* of activation amplitudes in response to task  $k$ ,  $\boldsymbol{\beta}_k = (\beta_{1k}, \dots, \beta_{Nk})' \in \mathbb{R}^N$ , as a latent field across the  $N$  data locations, and assuming a spatial prior to incorporate prior knowledge of local spatial dependence and sparsity [Zhang et al., 2015]. The surface-based spatial Bayesian GLM proposed by Mejia et al. [2020b] makes use of a particular class of Gaussian Markov Random Field (GMRF) priors called stochastic partial differential equation (SPDE) priors, which approximate a continuous Matérn random field by a GMRF [Lindgren et al., 2011, Bolin and Lindgren, 2013]. SPDE priors are built on a triangular mesh (see Appendix **Figure A.2**), the format of cortical surface data. An SPDE prior for a given Gaussian process  $\boldsymbol{\beta}$  takes the form

$$\boldsymbol{\beta} = \boldsymbol{\Psi} \mathbf{w}, \quad \mathbf{w} \sim \text{Normal}(\mathbf{0}, \mathbf{Q}_{\kappa, \tau}^{-1}), \quad (2)$$

$$\mathbf{Q}_{\kappa, \tau} = \tau^2 (\kappa^4 \mathbf{C} + 2\kappa^2 \mathbf{G} + \mathbf{G} \mathbf{C}^{-1} \mathbf{G}), \quad (3)$$

where  $\boldsymbol{\Psi}$  is an  $N \times n$  indicator matrix mapping the  $N$  data locations to  $n$  mesh locations. The mesh may contain additional locations to satisfy shape and size constraints and boundary locations to improve estimation along the data boundary. In the SBSB GLM, additional mesh locations consist of the medial wall, which serves as a supplemental layer to improve estimation along the data boundary. The matrix  $\mathbf{Q}_{\kappa, \tau}$  is a sparse precision (inverse covariance) matrix with a fixed set of non-zero elements whose value are determined by  $\kappa$  and  $\tau$ , parameters that control the smoothness and variance of the latent field. The matrix  $\mathbf{G}$  is a sparse, symmetric adjacency matrix in which non-zero entries exist only on the diagonal and in cells corresponding to neighboring locations, and  $\mathbf{C}$  is a diagonal matrix [Bolin and Lindgren, 2013].

The single-run SBSB GLM assumes independent SPDE priors on each of the  $K$  latent fields. Let  $\mathbf{y} = (\mathbf{y}'_1, \dots, \mathbf{y}'_N)' \in \mathbb{R}^{NT \times 1}$ , let  $\mathbf{X} = \text{block-diagonal}(\mathbf{X}_1, \dots, \mathbf{X}_N) \in \mathbb{R}^{NT \times NK}$ , and let  $\boldsymbol{\beta} = (\boldsymbol{\beta}'_1, \dots, \boldsymbol{\beta}'_N)' \in \mathbb{R}^{N \times K}$ . The surface-based spatial Bayesian GLM is given by

$$\begin{aligned} \mathbf{y} | \boldsymbol{\beta} &= \mathbf{X} \boldsymbol{\beta} + \mathbf{e}, \quad \mathbf{e} \sim \text{Normal}(\mathbf{0}, \sigma^2 \mathbf{I}_{NT}) \\ \boldsymbol{\beta}_k &= \boldsymbol{\Psi} \mathbf{w}_k, \quad \mathbf{w}_k | \kappa_k, \tau_k \sim \text{Normal}(\mathbf{0}, \mathbf{Q}_{\kappa_k, \tau_k}^{-1}), \quad k = 1, \dots, K \\ \boldsymbol{\theta} &= (\kappa_1, \tau_1, \dots, \kappa_K, \tau_K, \sigma^2) \sim \pi(\boldsymbol{\theta}), \end{aligned} \quad (4)$$

where  $\boldsymbol{\theta}$  contains all the model hyperparameters, and  $\pi(\boldsymbol{\theta})$  is their joint hyperprior.

**Multi-run model.** If multiple runs of task data are available from a given subject, it is beneficial to leverage those repeated measures to more accurately estimate the model hyperparameters (e.g. the parameters  $\kappa_k$  and  $\tau_k$  controlling the spatial properties of the activation amplitude for each task  $k$ , and the residual variance  $\sigma^2$ ). We therefore propose a multi-run spatial Bayesian GLM to jointly model runs  $j = 1, \dots, J$ . Let  $\mathbf{y}_j$ ,  $\mathbf{X}_j$ ,  $\boldsymbol{\beta}_j$ ,  $\boldsymbol{\beta}_{j,k}$ , and  $\mathbf{e}_j$  be the run  $j$ -specific quantities in equation (4). The multi-run SBSB GLM can be represented as

$$\begin{aligned} \mathbf{y}_j | \boldsymbol{\beta}_j &= \mathbf{X}_j \boldsymbol{\beta}_j + \mathbf{e}_j, \quad \mathbf{e}_j \sim \text{Normal}(\mathbf{0}, \sigma^2 \mathbf{I}_{NT}), \quad j = 1, \dots, J \\ \boldsymbol{\beta}_{j,k} &= \boldsymbol{\Psi} \mathbf{w}_{j,k}, \quad \mathbf{w}_{j,k} | \kappa_k, \tau_k \sim \text{Normal}(\mathbf{0}, \mathbf{Q}_{\kappa_k, \tau_k}^{-1}), \quad k = 1, \dots, K \\ \boldsymbol{\theta} &= (\kappa_1, \tau_1, \dots, \kappa_K, \tau_K, \sigma^2) \sim \pi(\boldsymbol{\theta}). \end{aligned} \quad (5)$$

Note that the run-specific activation amplitudes,  $\boldsymbol{\beta}_{j,k}$ , are estimated individually, while sharing a common prior determined by the parameters  $\kappa_k$  and  $\tau_k$ . Additionally, the between-run average amplitude can be estimated. These provide more statistically efficient estimates of activation amplitudes if differences across runs are not of interest. These averages are constructed as linear combinations of the run-specific latent fields, so their posterior distribution is available and can be used to identify areas of activation as described in Section 2.1.3 below.

## 2.1.2 Group-level modeling

Previously proposed spatial Bayesian GLMs for volumetric fMRI data were limited to single-subject analysis, in large part due to the computational burden associated with analyzing data from many subjects concurrently. Mejia et al. [2020b] proposed a computationally efficient “joint” group-level modeling approach based on first estimating each subject-level model separately, and then combining the results in a principled way. Here, we generalize this approach to any number of runs,  $J \geq 1$ . For simplicity of notation, assume that all subjects have

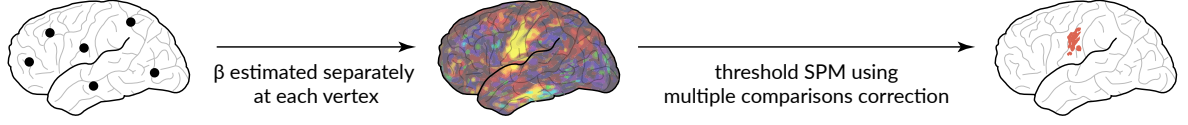
# General Linear Model (GLM)

$$\text{BOLD} = \text{Design} \times \begin{matrix} \text{Activation} \\ \text{Amplitude } (\beta) \end{matrix} + \text{Error}$$

1. Estimating activation amplitude ( $\beta$ )

2. Identifying areas of activation

Classical GLM



Spatial Bayesian GLM

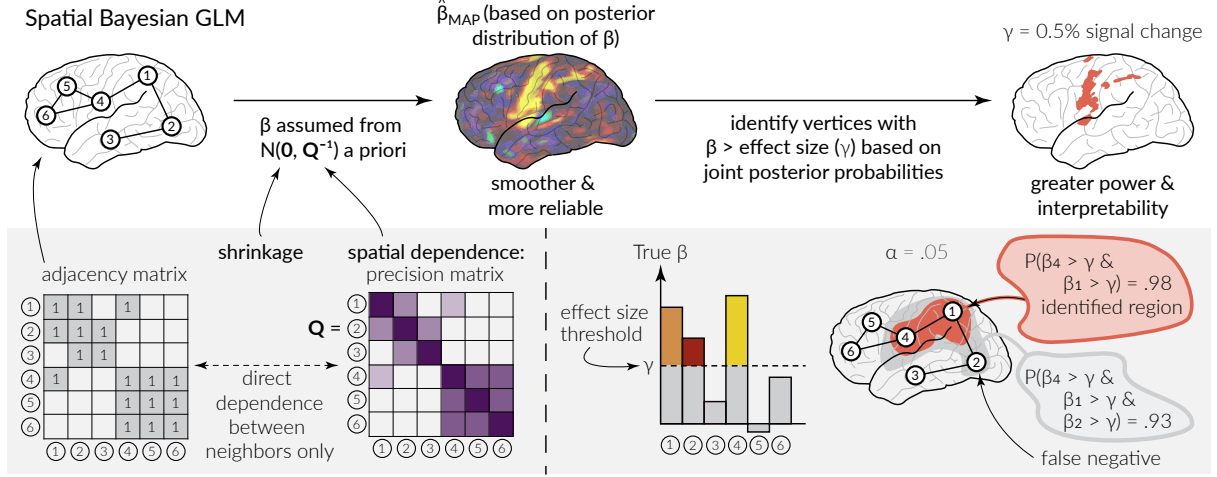


**Figure 1:** The surface-based spatial Bayesian GLM compared with the classical GLM. Both GLMs consist of two stages: (1) estimating activation amplitude and (2) identifying areas of activation. At stage 1, the Bayesian GLM incorporates spatial dependence and performs shrinkage of background locations through a prior on  $\beta$ , resulting in smoother and more reliable estimates of activation, given by the maximum-a-posteriori (MAP) value from the posterior distribution of  $\beta$ . At stage 2, the Bayesian GLM identifies the collection of vertices with activation amplitude above a specified effect size, based on joint posterior probabilities. This results in greater power to detect true activations.

the same number of runs  $J$ . Let  $\beta_m \in \mathbb{R}^{JKN}$  represent the activation amplitudes for subject  $m$  for all tasks and all runs. The joint group-level modeling approach is based on specifying a group-level contrast matrix  $\mathbf{A}$ , so that the quantity of interest can be expressed as a linear combination of the subject-level parameter estimates. Namely,  $\beta_G = \mathbf{A}\beta \in \mathbb{R}^N$ , where  $\beta = (\beta'_1, \dots, \beta'_M)' \in \mathbb{R}^{JKNM}$  is the concatenated activation amplitudes across all runs, subjects, and tasks. For example,  $\mathbf{A}$  can be constructed to represent the group average activation amplitude in response to a particular task, the difference in average amplitude across two groups of subjects or different conditions, or a contrast across tasks. Note that this group-level modeling would treat each run as if it were coming from a different subject unless used in conjunction with the multi-run subject analysis, which allows the different runs from the same subject to share the hyperparameters  $\theta = (\kappa_1, \tau_1, \dots, \kappa_K, \tau_K, \sigma^2)'$ . See Mejia et al. [2020b] for details on the posterior computation of  $\beta_G$ . Having obtained its posterior distribution, the estimate of  $\beta_G$  is given by its posterior mean or other summary metric, and we can identify group-level areas of activation as described in the following section.

## 2.1.3 Identifying areas of activation

In the SBSB GLM, areas of activation are identified based on the joint posterior distribution of activation across all locations using an excursions set approach [Bolin and Lindgren, 2015], implemented in the **excursions** R package [Bolin and Lindgren, 2018]. This approach avoids massive multiple comparisons and the need for multiplicity correction. As a result, power is increased relative to both the classical GLM and previously proposed spatial

Bayesian models, which used the marginal posterior distribution at each location to identify areas of activation and hence required multiplicity correction.

In the classical GLM, by contrast, areas of activation in response to each task or stimulus are typically identified by performing a  $t$ -test at every vertex, followed by correction for multiple comparisons. Multiplicity correction typically aims to control the family-wise error rate (FWER) or the false discovery rate (FDR) [Benjamini and Hochberg, 1995]. Many techniques have been proposed to account for spatial dependence and encourage spatial contiguity at the correction stage, including permutation tests, random field theory [Poline et al., 1997], and threshold-free cluster enhancement [Smith and Nichols, 2009]. However, these techniques are limited by the shortcomings of massive univariate modeling at the model estimation stage, and as a result will have reduced power to detect activations. The correction itself has the effect of further diminishing power to detect activations.

Since in the SBSB GLM spatial dependence is accounted for and leveraged at both estimation and inference, its power to detect activations tends to be quite high. This can result in large areas of activation with small but non-zero effect size being identified. To avoid this, it is common to specify a scientifically relevant activation threshold,  $\gamma$ , above which activations are of interest. For example, if the data are scaled to represent percent signal change, an activation threshold of  $\gamma = 0.5\%$  to  $2\%$  may be reasonable, depending on the magnitude of signal change evoked by a particular task. For a given value of  $\gamma$  and significance level  $\alpha$ , the areas of activation identified can be said to have activation greater than or equal to  $\gamma$  with probability at least  $1 - \alpha$ , based on the joint posterior distribution across all vertices. That is, there is probability of  $\alpha$  or less that at least one vertex in the activated region is a false positive. The excursions set approach therefore controls the FWER at level  $\alpha$ , but with typically much greater power to detect true activations than in the classical GLM.

## 2.2 Data and Model Estimation

### 2.2.1 Data Collection

We perform an extensive reliability study using cortical surface task fMRI data from the Human Connectome Project (HCP) [Van Essen et al., 2013, Barch et al., 2013]. To compare the reliability of estimates and areas of task activation produced using the SBSB GLM with the classical GLM, we analyze 180 task fMRI runs from 45 subjects who participated in the Human Connectome Project (HCP) and the HCP Retest Dataset. The sample of 45 subjects included 31 females, with 4 subjects between the ages of 22 and 25, 14 subjects between the ages of 26 and 30, and 27 subjects between the ages of 31 and 35. Each subject was scanned while performing a motor task [Barch et al., 2013]. The study used a 3-second visual cue to alert the subject of the type of motor task that they were expected to complete. Subjects were instructed to tap their fingers (left or right hand), squeeze their toes (left or right foot), or move their tongue for 12 seconds after being prompted by the cue. Each of the five motor tasks was repeated twice during each run. Two runs (acquired with opposing LR and RL phase-encoding directions) were collected at each of two visits, resulting in four runs per subject.

### 2.2.2 Preprocessing and Prewhitening

The task fMRI data was preprocessed according to the HCP minimal surface preprocessing pipelines, including projection to the cortical surface and registration to a common surface template [Glasser et al., 2013]. These pipelines also include generation of a subject-specific high-resolution 164k native surface mesh based on the high-resolution T1-weighted and T2-weighted structural images for each subject, registration to the *fsaverage* mesh, and resampling to a lower-resolution 32k mesh to approximately match the original fMRI voxel resolution. For spatial modeling we utilize the *midthickness* surface, which represents the midpoint of the cortical ribbon between the white matter and pial surfaces. As part of the HCP minimal preprocessing pipelines, the fMRI timeseries were slightly smoothed along the midthickness surface to regularize the mapping process using a 2mm full-width half-maximum (FWHM) Gaussian kernel. However, no additional spatial smoothing was performed prior to model estimation in our analyses.

Prior to model estimation, several additional processing steps are performed: resampling, centering and scaling, nuisance regression, and prewhitening. First, each surface is resampled from approximately 32,000 vertices to approximately 5,000 vertices per hemisphere using barycentric interpolation, which minimizes blurring [Glasser et al., 2013]. This greatly improves computational efficiency for the SBSB GLM, as well as for the vertex-wise prewhitening employed in both the SBSB and classical GLMs, which we describe below. After resampling, vertex size remains small relative to the size of expected activations. Notably, the interpolation is much less extreme than that introduced by spatial smoothing at even modest levels (e.g. 5mm FWHM).

The BOLD timeseries at each vertex and each column of the design matrix is centered prior to model fitting. This eliminates the need for a baseline field, since the intercept of a linear model is zero when both each predictor and the response have mean zero. The BOLD timeseries at each vertex is also simultaneously scaled relative to the local average BOLD signal, which introduces units of percent signal change. The task design matrix is created by convolving the stimulus boxcar function with a canonical double-Gamma HRF [Friston et al., 1998, Glover, 1999]. Twelve motion covariates (six rigid body realignment parameters and their first derivatives), along with linear and quadratic drift terms, are regressed from the BOLD data and task design matrix. Simultaneously with nuisance regression, the temporal derivative of each task design column is also regressed from the data and design matrix, in order to account for differences in the onset of the hemodynamic response across subjects, runs, tasks and areas of the brain.

Prewhitening is performed to satisfy the GLM assumption of residual independence. Prewhitening at vertex  $v$  consists of estimating the residual covariance matrix  $\Sigma_v$ , then pre-multiplying the BOLD data and design matrix by  $\Sigma_v^{-\frac{1}{2}}$ . This induces a residual vector that is temporally independent and residual variance that is constant across all vertices. To estimate  $\Sigma_v$ , we first estimate the residuals at vertex  $v$  using the classical GLM after performing the processing steps described above. We elect to use a high-order, spatially-varying autoregressive (AR) process to model the residual autocorrelation, since both are observed to be necessary based on exploratory analysis of the residuals (see Appendix **Figure B.3**). Specifically, an AR(6) model is fit to the each residual timeseries using the Yule-Walker equations [Brockwell et al., 2016]. To regularize the estimates, the estimated AR coefficients and white noise variance are averaged runs in the multi-run model for each subject and visit, and surface-smoothed using a Gaussian kernel with a FWHM of 6mm (see Appendix **Figure B.3**). The resulting AR coefficient and white noise variance estimates at each vertex  $v$  are used to compute  $\Sigma_v^{-\frac{1}{2}}$ . This vertex-wise procedure results in a unique design matrix at each vertex, as in equation (1).

### 2.2.3 Model Estimation

For each subject and visit, estimates and areas of activation are produced using the multi-run SBSB GLM described in Section 2.1.1. For comparison, the single-run SBSB GLM results are also obtained based on the LR runs. The two visits are analyzed independently to assess the test-retest reliability of the estimates and areas of activation. Since the surface meshes representing the left and right hemispheres do not intersect, each hemisphere is estimated separately in the Bayesian GLM. For both the classical and Bayesian GLMs, lateralized tasks (e.g. left foot, right hand) are excluded in the model for the ipsilateral hemisphere, since minimal ipsilateral activation is expected during lateralized motor tasks. Mejia et al. [2020b] found that this approach is computationally advantageous for Bayesian modeling, while having negligible impact on model results.

For each subject- and visit-specific model, areas of activation are identified using a significance level of  $\alpha = 0.01$  at three different activation thresholds,  $\gamma = (0\%, 0.5\%, 1\%)$  using the excursions set approach described in Section 2.1.3. Using a range of activation thresholds allows identification of areas that exhibit even subtle activation separately from those that exhibit high levels of activation in response to each task. Subject-level activations are identified for each run and for the average across runs for each visit.

For the classical GLM, areas of activation are identified by performing a  $t$ -test at each vertex, and using Bonferroni correction to control the FWER at  $\alpha = 0.01$ . While Bonferroni correction is often considered overconservative in a volumetric or full-resolution surface analysis, note that here the correction is only performed across approximately 5,000 resampled vertices within each hemisphere, and will therefore be much less conservative. As described in Section 2.1.3, FWER correction provides similar false positive rate guarantees as the excursions set approach adopted in the SBSB GLM. Correction is performed within each hemisphere to provide analogous false positive control to the Bayesian GLM. Though traditionally the classical GLM implicitly assumes an activation threshold of 0%, corresponding to the traditional hypothesis testing approach, here we test all three activation thresholds ( $\gamma = (0\%, 0.5\%, 1\%)$ ) to provide an apples-to-apples comparison with the areas of activation produced via the Bayesian GLM.

We applied the joint group-level modeling approach described in Section 2.1.2 to obtain estimates of group-average activation amplitude across all 45 subjects. Each visit is analyzed independently to facilitate reliability analysis. We also assess the impact of sample size on reliability of group-level estimates and areas of activation, since smaller sample sizes are relatively common in fMRI studies. To this effect, the group-level modeling is repeated on random subsets of 10, 20, and 30 subjects; for each sample size, ten different random samples of subjects are generated and analyzed. Areas of activation are identified as in the single-subject case for both the classical and Bayesian GLMs.

We fit the subject- and group-level Bayesian and classical GLMs using the R package `BayesfMRI` (version 1.8) running on 6 parallel threads on a Mac Pro with a 2.7 GHz 24-Core Intel Xeon W processor and 512 GB of memory. The `BayesfMRI` package is openly available via Github<sup>1</sup> and performs model fitting using the `R-INLA` package [Lindgren and Rue, 2015] with the `PARDISO` sparse matrix library [Alappat et al., 2020, Bollhöfer et al., 2020, 2019]. In sum, 180 subject-level models are fit (45 subjects, 2 visits, 2 hemispheres). Each model required approximately 86 minutes (sd 18 minutes) to complete, including resampling and other preprocessing steps, prewhitening, and model fitting. Computation times for group-level model estimation, including areas of activation, are shown in Table 1.

Subset Size	Runtime (min)
	median (SD)
10	41.48 (8.84)
20	80.79 (58.24)
30	124.84 (49.15)
45	170.46 (50.65)

**Table 1:** Computation time of group-level Bayesian model estimation based on pre-computed subject-level Bayesian models. For each subset size, the median and standard deviation (SD) across subsets, hemispheres and visits is reported.

## 2.3 Reliability analysis

The SBSB GLM leverages spatial dependence and sparsity to produce estimates and areas of activation that should, in theory, more accurately reflect the true underlying patterns of activation. Here, we assess the ability of the SBSB GLM to deliver on that promise. We assess the extent to which the SBSB GLM produces estimates and areas of activation that reflect the unique activation features of individual subjects. To this end, we utilize the repeated visits available for each subject, which are analyzed independently as described in Section 2.2.3. We use three types of metric to quantify reliability of subject-level measures of task activation: (1) intraclass correlation coefficient of estimates of activation amplitude, which quantifies the proportion of variability on the estimates attributable to unique and reliable subject-level features, (2) similarity of estimates to an unbiased ground truth proxy, and (3) test-retest overlap of areas of activation. At the group-level, we also use the similarity of estimates to an unbiased ground truth proxy to assess reliability. Finally, we assess power based on the size of areas of activation.

### 2.3.1 ICC of Amplitude Estimates

To quantify reliability of amplitude estimates, we compute the intraclass correlation coefficient (ICC) [Bartko, 1966] at each vertex  $v$  for each task, based on all 45 subjects and both visits. We compute the ICC for the LR and RL runs, as well as for the cross-run average. The ICC is equal to  $ICC = \sigma_b^2 / \sigma_t^2$ , where  $\sigma_b^2$  is the between-subject (signal) variance and  $\sigma_t^2 \geq \sigma_b^2$  is the total variance, equal to the sum of the between-subject variance and the within-subject (noise) variance  $\sigma_w^2$ . If a set of estimates are structured as  $\mathbf{B} \in \mathbb{R}^{M \times 2}$ , where  $M$  is the number of subjects and the two columns correspond to repeated measurements, the variance components can be computed as

$$\sigma_t^2 = \frac{1}{2} (\text{var}(\mathbf{B}_{\bullet,1}) + \text{var}(\mathbf{B}_{\bullet,2})), \quad \sigma_w^2 = \frac{1}{2} \text{var}(\mathbf{B}_{\bullet,1} - \mathbf{B}_{\bullet,2}), \quad \sigma_b^2 = \sigma_t^2 - \sigma_w^2,$$

where  $\mathbf{B}_{\bullet,j}$  indicates the set of estimates from all subjects for measurement  $j$  and  $\text{var}(\mathbf{x}) = \frac{1}{n} \sum_{i=1}^n (x_i - \bar{x})^2$ .

The interpretation of ICC is straightforward: a value of 1 happens when  $\sigma_t^2 = \sigma_b^2$ , which indicates that there is no noise present in the amplitude estimates for a given subject; a value of 0 happens when  $\sigma_b^2 = 0$ , which indicates that there are no true differences between subjects, and all observed differences in a set of estimates are due to random noise.

Note that negative ICC values are computationally possible given the estimation of  $\sigma_b^2$  as a difference, especially when the true ICC is close to zero. In activation amplitudes, this occurs most commonly outside of the areas of activation for a given task, where all subjects have essentially zero activation. Since ICC truly ranges from 0 to 1, we truncate any negative values to zero.

<sup>1</sup><https://github.com/mandymejia/BayesfMRI/tree/1.8>

### 2.3.2 Similarity of Amplitude Estimates to a Ground Truth

To assess the accuracy of subject-level amplitude estimates, we use the visit 2 classical GLM estimates as a proxy for the ground truth for each subject. Note that the classical GLM is used as the ground truth proxy for both the Bayesian and classical GLMs, providing two benefits: it is unbiased (though noisy), and it is common to both GLMs, avoiding any bias in favor of the Bayesian GLM. To quantify the similarity of estimates to this ground truth, we compute the mean squared error (MSE) and Pearson correlation for the visit 1 estimates, relative to this reference. Lower MSE and higher Pearson correlation indicate better accuracy.

We take a similar approach to quantify the accuracy of group-level estimates of activation amplitude. In that case, the visit 2 group-average estimates of activation based on the classical GLM are used as a proxy for the ground truth.

### 2.3.3 Overlap of Activations

To quantify the reliability of areas of activation produced from the Bayesian and classical GLMs, we utilize the Dice overlap coefficient [Dice, 1945]. Dice of two binary maps  $A$  and  $B$  is given by the number of overlapping locations across the maps, divided by the average number of locations in each map.

$$Dice(A, B) = \frac{2|A \cap B|}{|A| + |B|}$$

For both the Bayesian and classical GLMs, we compute the Dice coefficient of test-retest overlap across visits for each subject at each activation threshold. We compute the test-retest overlap of both the run-specific areas of activation, as well as for the cross-run average areas of activation.

## 3 Results

In this section, we examine the reliability of subject-level and group average estimates and areas of activation. Using the classical GLM as a benchmark, we provide visual illustrations and summary measures of the gain in reliability attained using the Bayesian GLM. We also examine the power of both the classical and Bayesian GLM to identify areas of activation in individual subjects and at the group level. Unless otherwise stated, results shown are based on the multi-run analyses of the visit 1 data, combining across the LR and RL runs.

### 3.1 Subject-level estimates of activation amplitude

For three example subjects, **Figure 2** displays Bayesian and classical GLM estimates of activation amplitude for the tongue movement task. A corresponding figure for the amplitude estimates resulting from the analysis using only the LR run can be seen in Appendix **Figure D.5**. The remaining motor tasks and the visual cue multirun estimates for subject A are shown in Appendix **Figure D.6**. The Bayesian GLM produces estimates that are much smoother, without noticeably oversmoothing the areas of highest activation, shown in yellow. In addition, the unique individual patterns of functional activation are more clearly delineated in the Bayesian GLM. Compared with the single-run estimates, the multi-run average estimates are smoother for both the classical GLM and Bayesian GLM.

We quantify the test-retest reliability of the estimates of activation amplitude via the ICC, as described in section 2.3.1. Commonly-used ICC quality thresholds were established by Cicchetti [1994]: ICC below 0.4 is considered “poor”, ICC between 0.4 and 0.6 is considered “fair”, ICC between 0.6 and 0.75 is considered “good”, and ICC over 0.75 is considered “excellent”. In **Figure 3**, we summarize the ICC of each image based on the proportion of vertices where fair, good and excellent ICC is achieved. Maps of the vertex-wise intraclass correlation coefficient (ICC) for each task are also shown in Appendix **Figure D.8**. Across all tasks, the proportion of vertices exhibiting fair or better ICC is higher based on the Bayesian GLM compared with the classical GLM. The proportion of vertices exhibiting good or better ICC is also higher based on the Bayesian GLM for most tasks. The proportion of vertices exhibiting excellent ICC is very small regardless of modeling strategy. These results illustrate that the Bayesian GLM produces estimates that are more reflective of reliable patterns of functional activation in individual subjects at the vertex level.

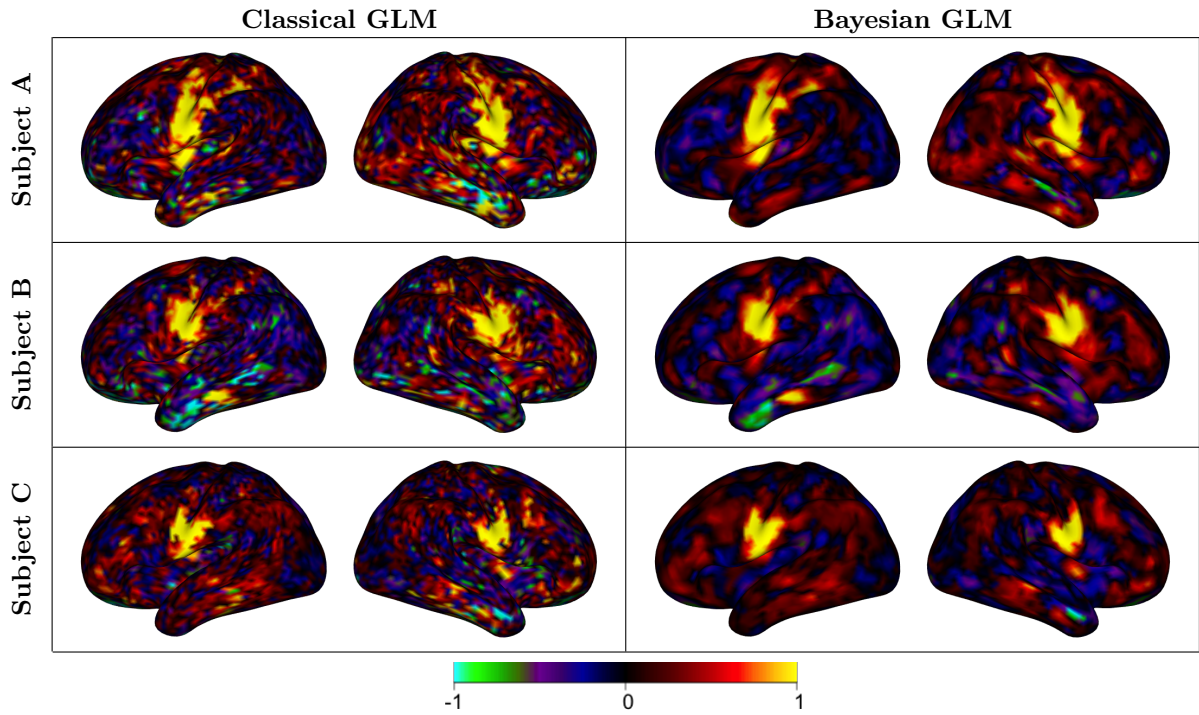


**Figure 2:** Subject-level estimates of activation amplitude in response to tongue movement, in units of percent signal change. For the sake of space, only the lateral view of each hemisphere is displayed. The Bayesian estimates are much smoother but are not noticeably oversmoothed in the areas of peak activation (shown in yellow). In addition, the unique individual patterns of functional activation are more clearly delineated in the Bayesian GLM. Compared with the single-run estimates, the multi-run average estimates are smoother for both the classical GLM and Bayesian GLM.



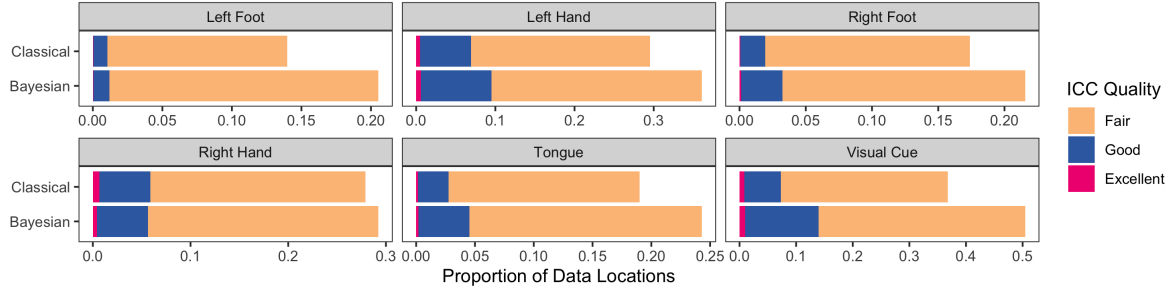


**Figure 3: Test-retest reliability of subject-level estimates of activation amplitude, in terms of ICC.** Each bar shows the proportion of vertices with estimates significantly greater than zero in the group analysis of the Bayesian result with “fair” (0.4 to 0.6), “good” (0.6 to 0.75) and “excellent” (over 0.75) ICC values, based on the independent estimates of activation from each visit. For each task, the proportion of vertices exhibiting fair or better ICC is higher based on the Bayesian GLM compared with the classical GLM. The proportion of vertices exhibiting good or better ICC is also higher based on the Bayesian GLM for most tasks. Note that the proportion of data locations with fair or better ICC values is much higher for the visual cue, suggesting that these results are much more consistent. This is likely an effect of having many more visual cues shown during a run than the number of times a specific motor task is performed. These results show that the Bayesian GLM produces more unique and reliable patterns of activation in individual subjects compared to the classical GLM

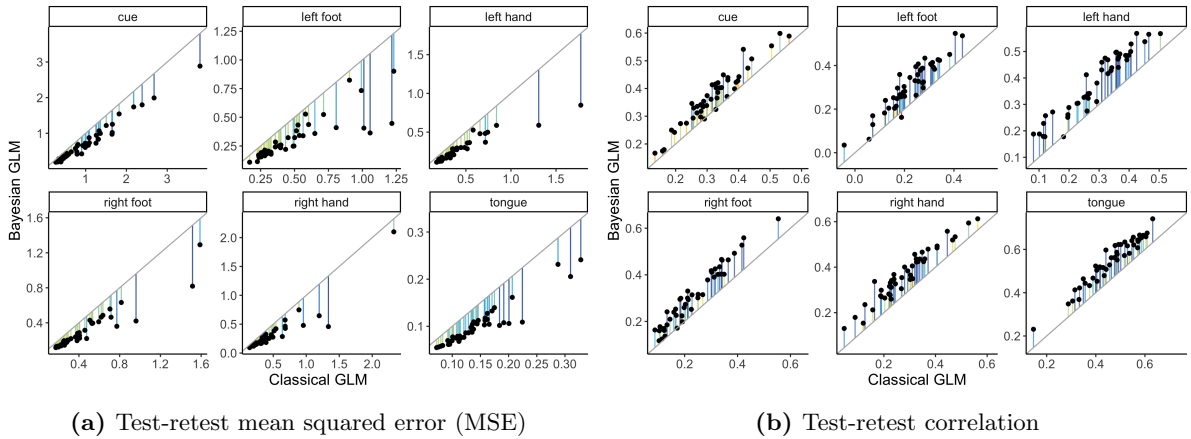


**Figure 4: Test-retest reliability of subject-level estimates of activation amplitude, in terms of test-retest MSE and correlation.** We used the *classical GLM* visit 2 amplitude estimates as a noisy but unbiased proxy for the truth to compute MSE and correlation. This avoids any bias in favor of the Bayesian GLM but will tend to result in equally inflated MSE and underestimated correlation for both GLMs. Both panels show that the classical and Bayesian GLMs tend to produce substantially more reliable estimates of activation with repeated runs. However, the Bayesian GLM consistently outperforms the classical GLM in terms of both test-retest mean squared error (MSE) and test-retest correlation. Across all tasks, *all* 45 subjects exhibit improved (reduced) test-retest MSE using the SBSB GLM. The vast majority of subjects exhibit improved (higher) test-retest correlation using the SBSB GLM, while a handful exhibit a negligible change. For each subject, line segments represent the magnitude of improvement in reliability using the SBSB GLM over the classical GLM.

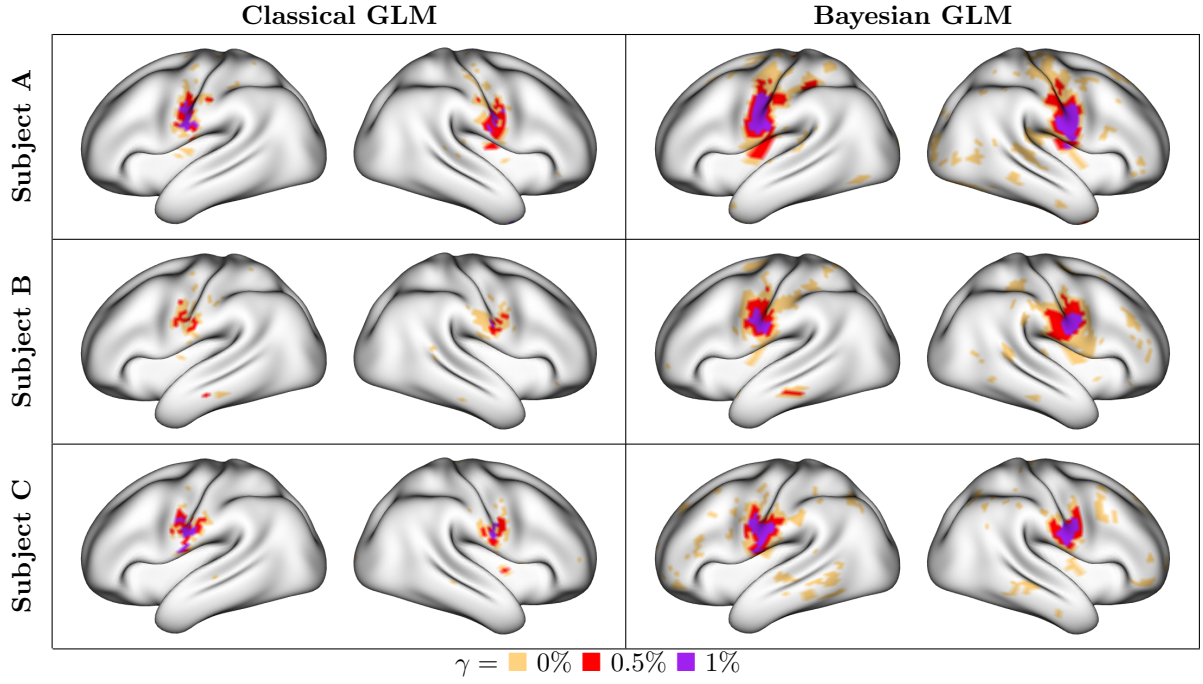


**Figure 5: Subject-level areas of activation during tongue movement.** For the sake of space, only the lateral view of each hemisphere is shown. For the classical GLM, activations are found through the family-wise error rate; for the Bayesian GLM, areas of activation are based on the joint posterior distribution. For all activations, the significance level is  $\alpha = 0.01$ . In both the classical and Bayesian GLM, this is the probability of a single false positive among the activated vertices. Three activation thresholds are considered:  $\gamma = (0\%, 0.5\%, 1\%)$  signal change. Areas of activation at an activation threshold of 0% represent areas exhibiting greater-than-zero amplitude, which corresponds to the traditional hypothesis testing approach in the classical GLM. The Bayesian GLM areas of activation are substantially larger than classical GLM ones, suggesting increased power to detect activations while maintaining strict false positive control.

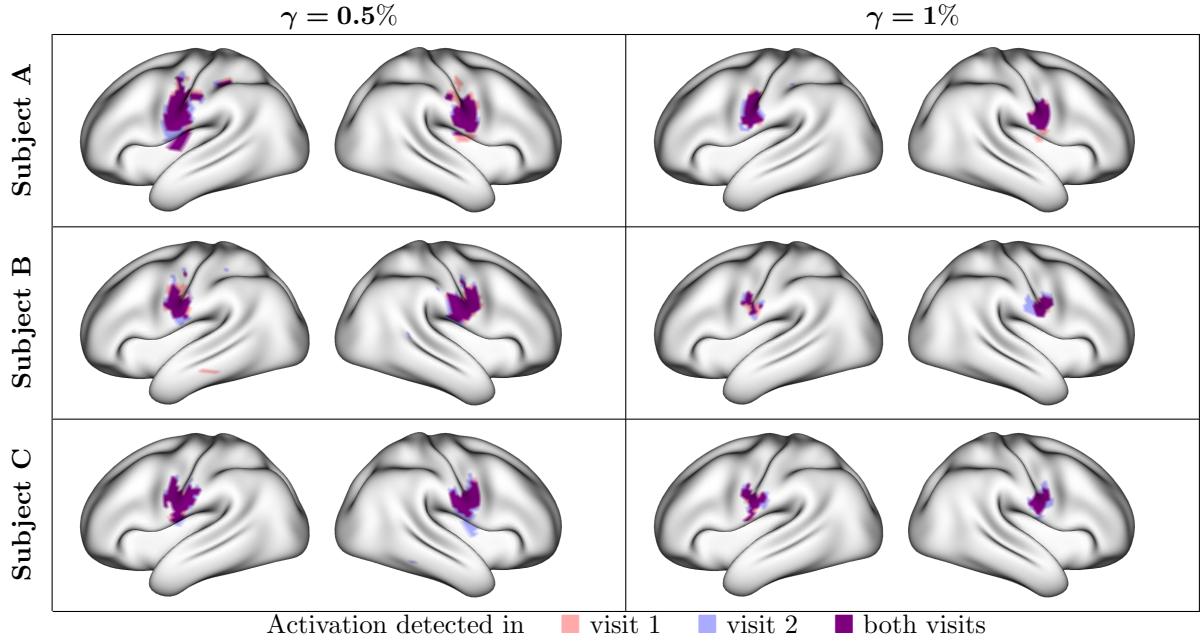


**Figure 6: Subject-level activations consistently detected across visits.** Areas of activation are found using the Bayesian GLM with activation thresholds  $\gamma = (0.5\%, 1\%)$  and significance level  $\alpha = 0.01$ . For the sake of space, only the tongue task and the lateral view of each hemisphere is shown. Areas of activation are highly consistent within each subject across visits. At the 0.5% threshold, areas of activation closely resemble the regions of peak activation amplitude observed in **Figure 2**.

**Figure 4** displays two additional metrics of test-retest reliability of estimates of activation amplitude, as described in Section 2.3.2: test-retest mean squared error (MSE) and test-retest correlation. Recall that since we do not know the true activation amplitude for each subject, we use the visit 2 *classical* amplitude estimates as a noisy but unbiased proxy for the truth. Note that we do not use the *Bayesian* amplitude estimates from visit 2 as the reference to avoid any bias in favor of the Bayesian GLM. It is important to note that the reference is a noisy proxy for the truth. However, any bias in the reference would tend to underestimate the reliability of the Bayesian and classical estimates equally.

**Figure 4a** displays the MSE of Bayesian versus classical estimates of activation. The Bayesian GLM produces universal reduction in test-retest MSE across all subjects and tasks. The largest reductions in MSE are seen in the subjects with the highest noise levels in the classical GLM. Test-retest correlation is shown in **Figure 4b** and largely agrees with the MSE result, with the vast majority of subjects showing improved correlation in the Bayesian GLM across different tasks. Together, these results suggest that the Bayesian GLM consistently produces more reliable subject-level estimates of activation amplitude.

In order to verify the robustness of the classical GLM using the resampled data, results are compared to full-resolution ( $\sim 32,000$  vertices per hemisphere) analysis using the classical GLM. The full-resolution classical GLM is performed on both unsmoothed data and data smoothed with a Gaussian kernel with a full-width half-maximum (FWHM) of 6mm. The performance of the classical GLM using the subject-level test-retest correlation with full-resolution smoothed data is similar to the resampled but unsmoothed data (See Appendix **Figure C.4**). Therefore, we conclude that resampling does not have a detrimental effect on the classical GLM.

### 3.2 Subject-level areas of activation

For the same three example subjects as above, **Figure 5** displays classical and Bayesian areas of activation for the tongue movement task. The remaining tasks for the multirun activations are shown in Appendix **Figures D.9** and **D.10**. Areas that show statistically significant activation *above* three activation thresholds ( $\gamma = 0\%$ ,  $0.5\%$  and  $1\%$ ) are displayed. The activation threshold  $\gamma = 0\%$  is analogous to a traditional hypothesis testing framework in the classical GLM, but is based on the joint posterior distribution of activation amplitude across all vertices. For both the classical and Bayesian GLMs, the significance level is set to  $\alpha = 0.01$ , which represents

an upper bound on the probability of observing a single false positive vertex, e.g. the FWER.

The most notable difference between the Bayesian and classical GLMs in **Figure 5** is that the Bayesian areas of activation are substantially larger at each activation threshold. Comparing with the estimates of activation amplitude for the same subjects shown in **Figure 2b**, the Bayesian GLM areas of activation above  $\gamma = 0\%$  correspond well to both areas of intense and more subtle activation, while those exceeding  $\gamma = 0.5\%$  or  $1\%$  signal change correspond well to areas of peak activation shown in yellow in **Figure 2b**.

Appendix **Figure D.9** displays classical and Bayesian areas of activation based on a single run. In both the single-run and two-run scenarios, the Bayesian GLM detects dramatically more active data locations in areas localized around regions with higher amplitude estimates from both the classical GLM and the Bayesian GLM. In general, the classical GLM appears to be underpowered to detect activations at the subject level, whether a single run or two runs are analyzed.

For our three example subjects, **Figure 6** shows test-retest overlap of Bayesian areas of activation for the tongue task at thresholds of  $\gamma = 0.5\%$  and  $1\%$ . Areas displayed in dark purple correspond to overlap across both visits, while areas displayed in semi-transparent blue and red correspond to only a single visit. These overlaps show remarkably strong within-subject consistency of Bayesian areas of activation across visits. We also observe clear differences in the topology of activations between subjects, particularly at the  $\gamma = 0.5\%$  threshold. This suggests that while individuals react to stimuli in broadly similar regions, the extent and shape of their activations vary considerably. The Bayesian GLM appears able to discover these individualized patterns of functional activation, due to its high power and ability to leverage spatial dependencies at all stages of analysis.

**Figure 7** quantifies the test-retest reliability of areas of activation in terms of the Dice coefficient of overlap, described in Section 2.3.3. Panel (a) displays the test-retest overlap of the subject-level Bayesian and classical areas of activation. The average over subjects is shown, along with error bars indicating 95% bootstrap confidence intervals. Panel (b) shows the *size* of activations, in terms of the number of overlapping vertices across both visits, versus test-retest overlap.

The most reliable activations are produced with the Bayesian GLM using an activation threshold of  $0.5\%$ , achieving a Dice overlap of near or above  $0.6$  for all tasks. For the classical GLM, the most reliable activations tend to be produced at the standard activation threshold of  $0\%$ , which corresponds to the traditional hypothesis testing approach. A reference line indicates this scenario, which serves as a baseline. Note that while the Bayesian and classical GLMs sometimes produce activations with similar test-retest overlap (e.g. with the  $0\%$  activation threshold for the hand, foot and tongue tasks), the Bayesian areas of activation are substantially larger, as seen in panel (b). Overall, the Bayesian GLM produces areas of activation that are both larger and more reliable than the classical GLM in individual subjects.

### 3.3 Group-level estimates and areas of activation

The surface-based spatial Bayesian GLM can also produce group-level estimates and areas of activation in a computationally efficient way. Here, we assess the reliability and power of the group-level Bayesian GLM in comparison with the classical GLM.

**Figure 8** displays group-average estimates of activation amplitude and areas of activation for the tongue task, based on all 45 subjects' visit 1 data (Appendix **Figures D.11** and **D.12** show group-average estimates and activations for all tasks). Pooling data across a group of subjects in the classical GLM tends to combat the high levels of noise contaminating subject-level estimates. The group-level classical estimates of activation are indeed much smoother than the subject-level classical estimates shown in **Figure 2**. Yet compared with the Bayesian GLM, the classical GLM estimates still exhibit higher levels of noise.

More noticeably, the size of activations shown in the bottom panel of **Figure 8** are smaller in the classical GLM versus the Bayesian GLM, regardless of activation threshold. This suggests that the Bayesian GLM has higher power to detect activations even in group analysis with a moderate sample size. In fact, the power in the Bayesian GLM is sufficiently high that we see areas with small effect size being detected as statistically significant at the  $0\%$  threshold. The Bayesian areas of activation above  $0.5\%$ , on the other hand, closely resemble the peak areas of activation seen in the amplitude maps in red and yellow. The issue of small effect size when power is high is a known issue for very large sample sizes in the classical GLM, but here we observe this phenomenon in a moderately sized sample in the Bayesian GLM. This is reflective of the much higher power of the Bayesian GLM. It also illustrates the importance of specifying a threshold above which activations are scientifically meaningful.

**Figure 9** displays two measures of test-retest reliability for the group-level estimates of activation amplitude:

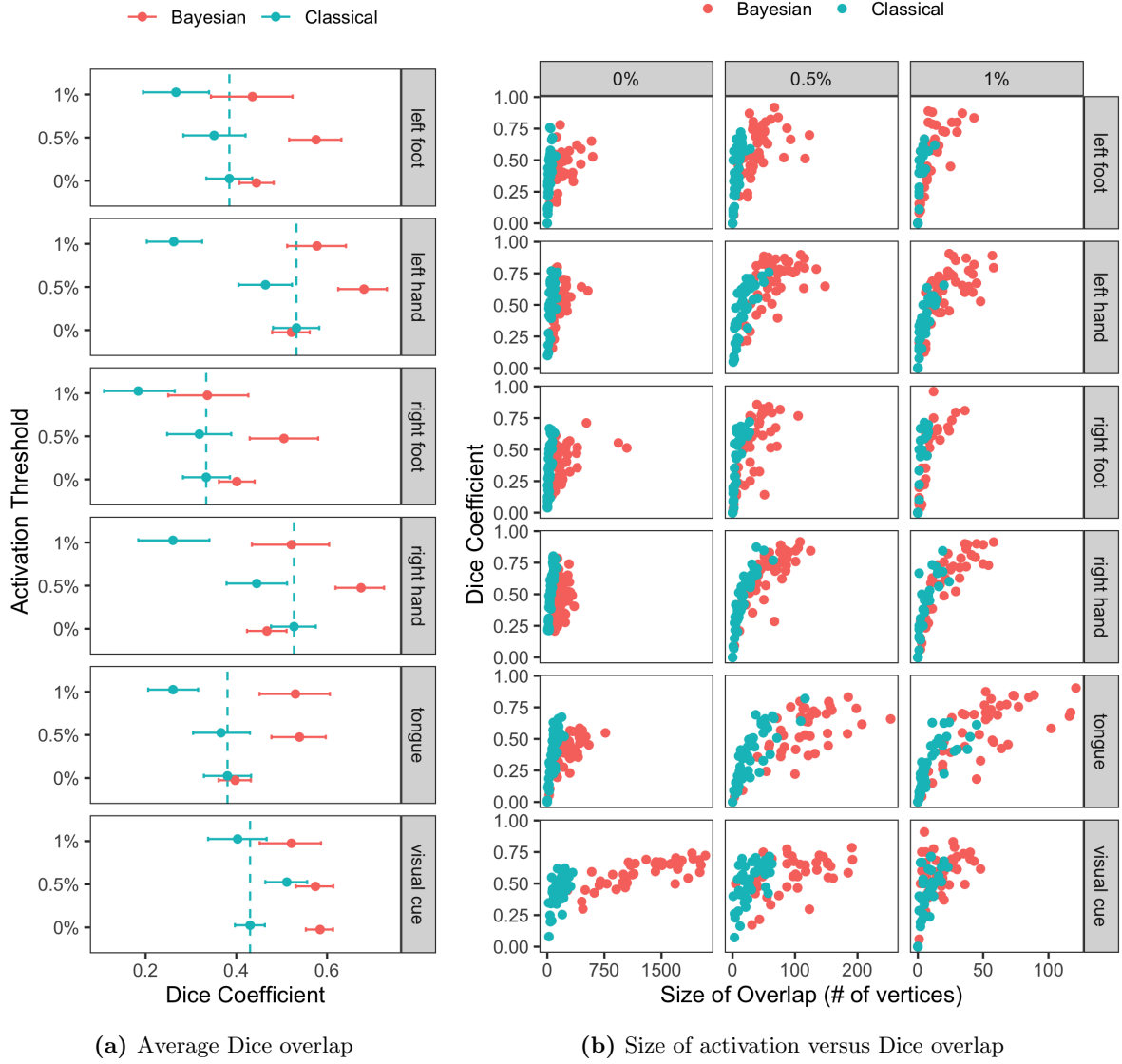


**Figure 7: Test-retest reliability of subject-level areas of activation.** Bayesian GLM areas of activation are based on the joint posterior distribution of activation amplitude across all vertices. Classical GLM areas of activation are based on performing a hypothesis test at every location and controlling the FWER. For both GLMs, the significance level is  $\alpha = 0.01$  within each hemisphere. **(a)** The average Dice test-retest overlap of areas of activation across all subjects, with 95% bootstrap confidence intervals. For the classical GLM, the most reliable areas of activation are typically produced using activation threshold  $\gamma = 0\%$ , corresponding to a traditional hypothesis-testing approach; this is treated as the benchmark and is indicated with a vertical line. For the Bayesian GLM, an activation threshold of  $\gamma = 0.5\%$  tends to produce the most reliable results, which significantly outperforms the classical GLM benchmark for all tasks. **(b)** Size of activation (overlap across both visits) versus Dice overlap. The Bayesian GLM produces areas of activation that tend to be both larger and more reliable. This illustrates that the Bayesian GLM benefits from both a gain in power, producing larger areas of activation, and a gain in reliability.

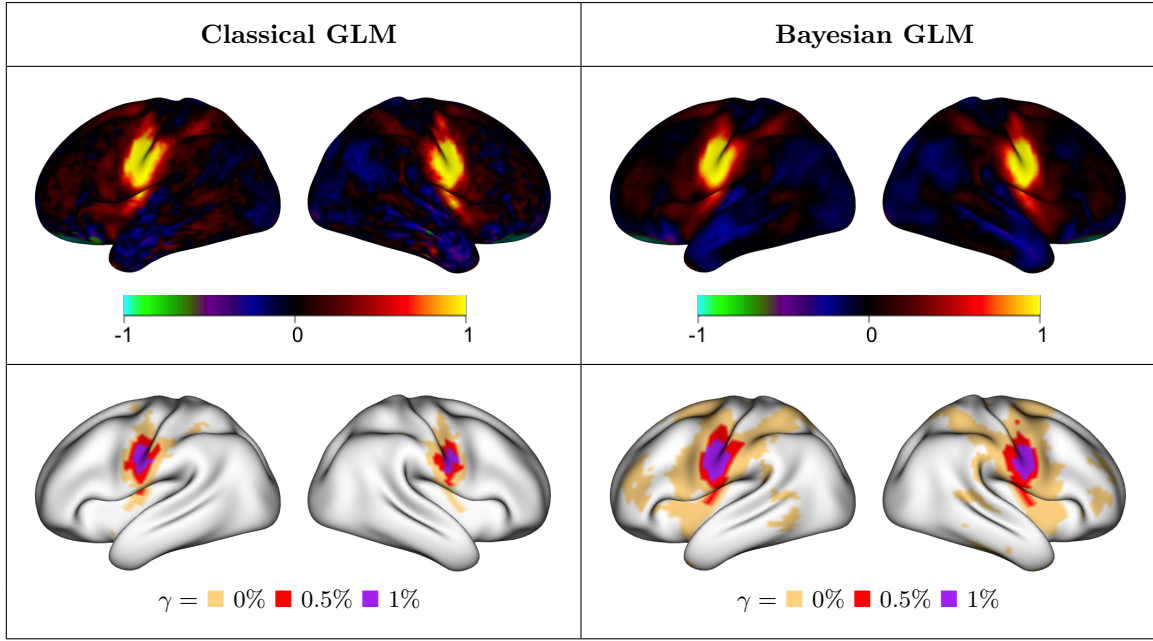


**Figure 8: Group-average estimates of activation amplitude (top) and areas of activation (bottom) for the tongue task.** Results are based on the average across 45 subjects. Higher levels of noise remain apparent in the classical GLM estimates of activation amplitude, despite the relatively large sample size. Areas of activation also remain smaller in the classical GLM versus the Bayesian GLM, suggesting reduced power to detect activations, even at the standard classical GLM hypothesis testing threshold of  $\gamma = 0\%$ .

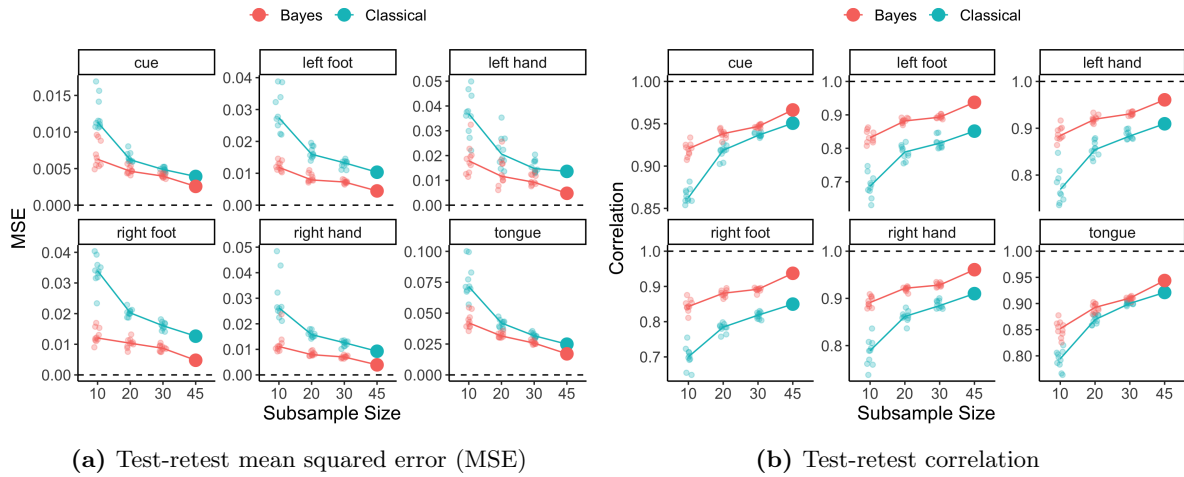


**Figure 9: Test-retest reliability of group-level estimates of activation amplitude, in terms of test-retest MSE and correlation.** Note that we used the *classical GLM* visit 2 group-level amplitude estimates as a noisy but unbiased proxy for the truth to compute MSE and correlation. This avoids any bias in favor of the Bayesian GLM but will tend to result in inflated MSE and underestimated correlation for both GLMs. Both panels show that the classical and Bayesian GLMs become more reliable as sample size increases. However, the Bayesian GLM consistently outperforms the classical GLM in terms of both test-retest mean squared error (MSE) and test-retest correlation, even for the full sample of 45 subjects.

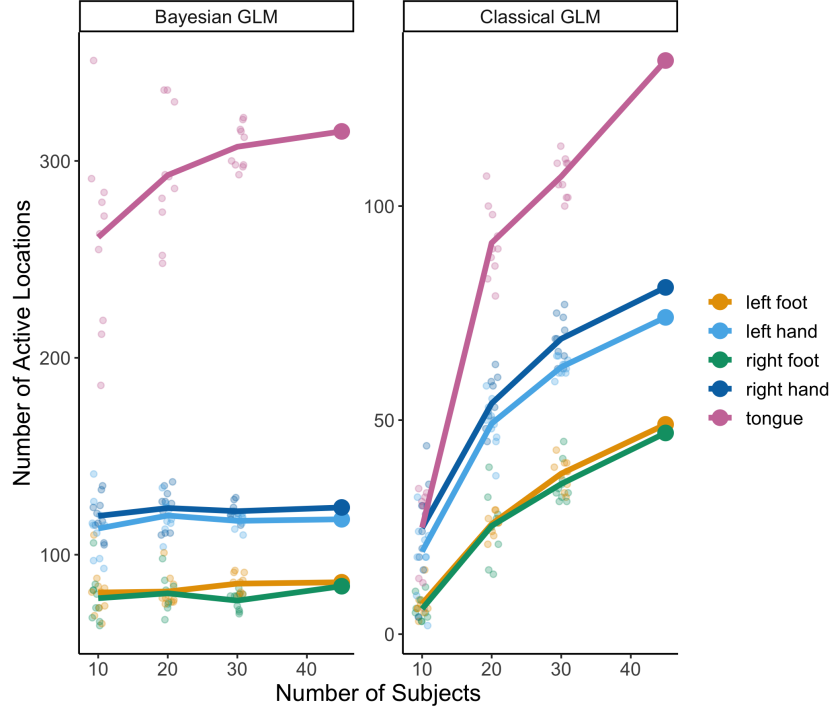


**Figure 10: Size of group-level areas of activation above 0.5% signal change.** Jittered dots represent random sub-samples of 10, 20 and 30 subjects; lines connect the averages within each sample size. The size of Bayesian activations is relatively flat across sample sizes, illustrating that the Bayesian GLM has high power to detect activations above 0.5% signal change even for small samples. The size of classical GLM activations is much smaller and continues to grow nearly linearly with increasing sample size, illustrating a lack of power in the classical GLM to detect activations, even with moderate sample size. The y-axis scales are intentionally allowed to vary, as the relative slopes are of greater interest than the comparison of absolute numbers.

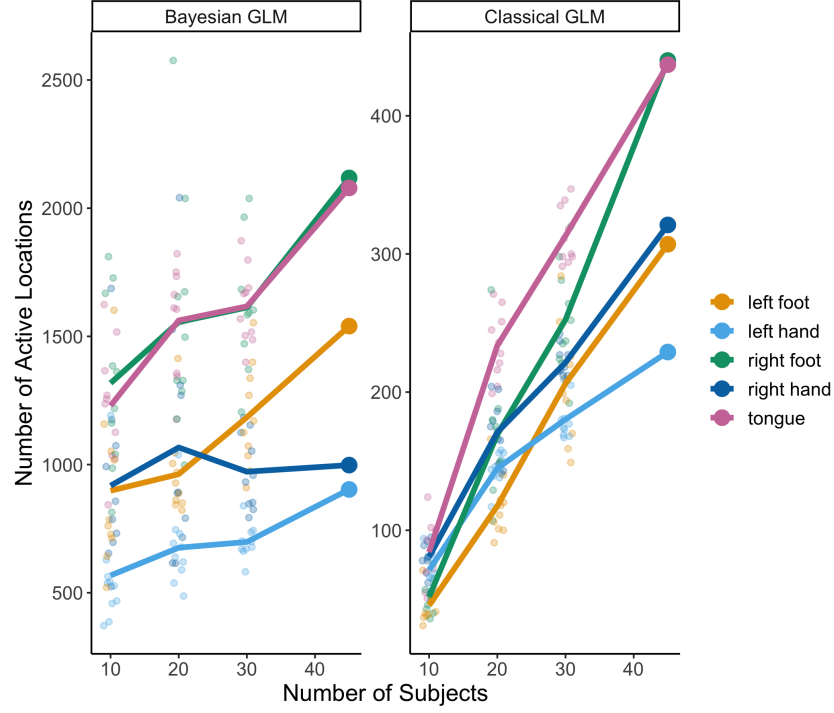


**Figure 11: Size of group-level areas of activation above 0% signal change.** Jittered dots represent random sub-samples of 10, 20 and 30 subjects; lines connect the averages within each sample size. The size of both the Bayesian and classical GLM activations grows with increasing sample size, but in the case of the Bayesian GLM many of these locations exhibit small effect size, which may not be of scientific interest. This illustrates the importance of considering effect size when identifying areas of activation, particularly when power is high as in the group-level Bayesian GLM. The y-axis scales are intentionally allowed to vary, as the relative slopes are of greater interest than the comparison of absolute numbers.



mean squared error (MSE) and correlation. Both measures are based on using the visit 2 *classical GLM* estimates of activation amplitude, providing a noisy but unbiased proxy for the unknown true activation amplitudes and avoiding any bias in favor of the Bayesian GLM. Note that this will tend to result in somewhat pessimistic measures of reliability, e.g. higher MSE and lower correlation, for both GLMs. Yet even so, the Bayesian GLM approaches perfect reliability (MSE of 0; correlation of 1) as sample size increases. For instance, the Bayesian GLM estimates of activation amplitude achieve test-retest correlation of approximately 0.95 across all tasks in the full sample of  $n = 45$  subjects.

**Figure 9** additionally shows that the Bayesian GLM achieves small-sample reliability similar to the reliability achieved by the classical GLM with much larger sample sizes. For the foot and hand motor tasks, for example, the Bayesian GLM test-retest reliability with a sample of  $n = 20$  is *better* (lower MSE, higher correlation) than of the classical GLM with  $n = 45$ , more than double the sample size. This illustrates that the group-level Bayesian GLM can extract more reliable measures of population activation from smaller samples compared with the classical GLM. Given the high cost of collecting larger samples, this illustrates an important benefit of the Bayesian GLM: it is able to extract maximal information from a sample, rivaling and perhaps even exceeding the benefit of doubling the sample size.

**Figures 10 and 11** further examine the power of the Bayesian GLM for different sample sizes. The size of group-level activations are shown as a function of sample size. When considering activations above 0.5% signal change (**Figure 10**), the size of Bayesian activations is relatively stable as sample size grows. This illustrates that the Bayesian GLM has high power to detect activations above 0.5% signal change even in very small samples. The size of classical GLM activations is much smaller and continues to grow nearly linearly with increasing sample size, reflecting a lack of power in the classical GLM to detect activations above a certain effect size, even with moderate sample size.

Using an activation threshold of 0% signal change (**Figure 11**), the size of both the Bayesian and classical GLM activations grows with increasing sample size. However, in the case of the Bayesian GLM these areas are quite large for some tasks (note that the total number of data locations is approximately 10,000). Many of these locations exhibit small effect size, which may not be of scientific interest. This illustrates the importance of considering effect size when identifying areas of activation, especially when power is high as in the Bayesian GLM.

Finally, we consider the relationship between the group-level and subject-level areas of activation, and what it implies about power at the individual subject level. First, note that *true* group-average activations should reflect some degree of *intersection* across true subject-level topologies of functional activation, which are unique and imperfectly overlapping. Locations that are only truly active in a small number of subjects are not likely to be “active” on average. Therefore, if our subject-level areas of activation are close to the truth (and not grossly underestimated due to lack of power), we would expect the size group-level areas of activation to likely be somewhat *smaller* than the largest subject-level activations. This may contradict the experience in practice, since the classical GLM tends to be underpowered at the individual subject level, producing very small areas of activation that do not reflect the true extent of activation.

**Figure 12** displays the size of subject-level and group-average Bayesian and classical areas of activation. For simplicity, only the activation threshold determined to be most reliable for each GLM, namely 0% for the classical GLM and 0.5% for the Bayesian GLM, are displayed (see **Figure 7a**). In the classical GLM, the group-average areas of activation are much larger than the subject-level areas of activation, reflecting lower power at the subject level. However, in the Bayesian GLM we indeed observe that the group-average size of activation is within the distribution of subject-level activation sizes. This is particularly true for the hand and foot tasks, where the group-average size of activation is close to the 75th percentile (the upper edge of the box) of the distribution of subject-level activation sizes. As describe above, this is consistent with what we would expect from the *true* areas of activation at the subject and group-average level. Though we can never estimate the truth perfectly, this suggests that even with a relatively small amount of data at the subject-level (four 12-second repetitions of each task over two runs), the Bayesian GLM has adequate power to detect unique functional features in individual subjects.

## 4 Discussion

The surface-based spatial Bayesian general linear model (GLM) leverages information shared between neighboring locations on the cortical surface to improve the accuracy of task amplitude estimates and to increase power to detect significant activations. We analyze test-retest motor task fMRI data from 45 subjects in the Human

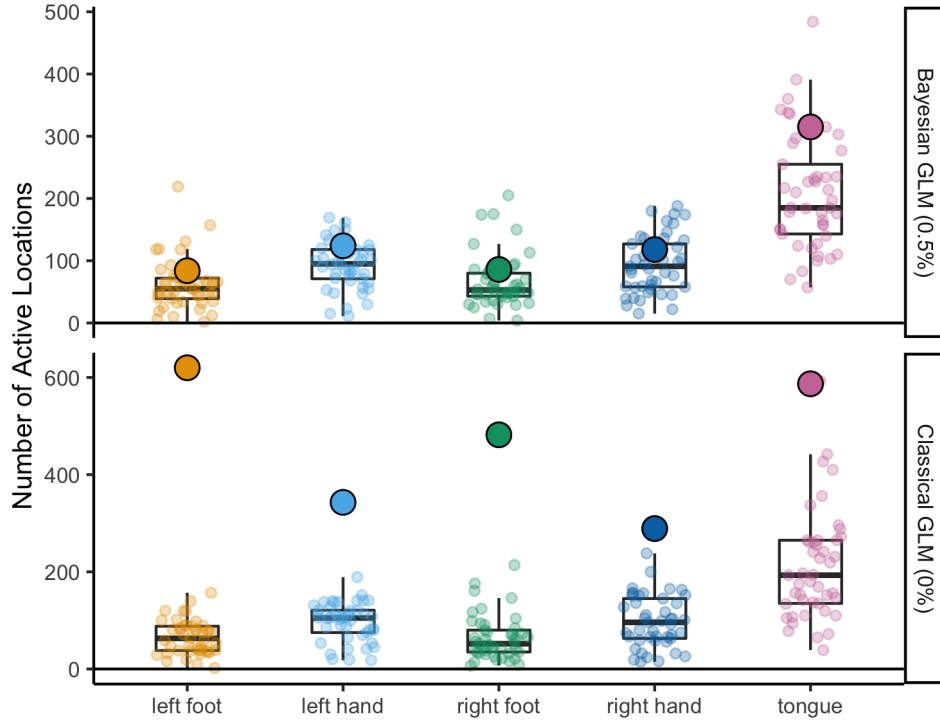


**Figure 12: Size of subject-level versus group-level activations.** Boxplots and jittered points indicate the size of each subject-level activations; filled circles indicate the size of group-average activations. For simplicity, we only display the most reliable activation threshold for each GLM (0.5% for the Bayesian GLM; 0% for the classical GLM) as shown in Figure 7(a). In the classical GLM, subject-level areas of activation are typically much smaller than group-level ones, suggesting a lack of power at the subject level. In the Bayesian GLM, group-level areas of activation better reflect the intersection across the unique patterns of subject-level activations

Connectome Project (HCP). Our findings establish that surface-based spatial Bayesian modeling produces more reliable subject-level and group-average estimates of activation amplitude and highly consistent subject-level areas of activation. We also observe a major gain in power over the classical GLM to detect activations in individuals and across groups of subjects. The Bayesian GLM is computationally efficient at both the subject and group level and is conveniently implemented in the R package `BayesfMRI`, facilitating the use of this approach to extract accurate and nuanced insights in future task fMRI studies.

## 4.1 Unique individual functional topology

We visualize estimates and areas of activation for several individual subjects to illustrate the effects of smoothness and noise reduction of the Bayesian GLM, but also to show the unique patterns of functional activation we observe in individuals using the Bayesian GLM. While these patterns are also visible using the classical GLM, they are somewhat obscured by high noise levels. More importantly, the Bayesian areas of activation above 0.5% signal change closely resemble the patterns of peak activation seen in the amplitude maps. Areas of activation produced using the classical GLM are not as representative of these patterns, due to low power at the subject level. We observe the Bayesian areas of activation to be highly similar across visits, suggesting that functional topology is a trait that can be consistently observed in individual subjects. Indeed, the within-subject test-retest overlap of activations is substantially higher than that of the classical GLM, achieving Dice coefficient as high as 0.7 for the left and right hand tasks. The ability to detect and quantify unique patterns of individual functional topology with relatively little data (e.g., four 12-second blocks of each motor task) is a valuable product of surface-based spatial Bayesian modeling. Such subject-level measures could be used to enhance understanding of differences in task performance across subjects, the manifestations of development or aging on functional topology, or the effects of disease progression or treatment on functional engagement.

## 4.2 Universally beneficial for subject-level analysis

We assess the ability of the Bayesian GLM to produce more reliable subject-level estimates of activation on average across subjects (using ICC) and in individual subjects (using test-retest MSE and correlation). We show a substantial increase in the number of brain locations exhibiting at least “fair” or “good” ICC. This illustrates that on average across subjects, the Bayesian estimates are more reflective of reliable features of individual subjects. Furthermore, analyzing the test-retest reliability at the individual subject level, we find that the Bayesian GLM produces more reliable estimates of activation across *every* subject included in our analysis.

The HCP includes two runs of motor task data (plus an additional two runs for the 45 subjects in the HCP retest dataset). This may not be the case for many more typical task fMRI studies, where often a single run may be collected for each subject. Therefore, we also examine the performance of the Bayesian GLM using only a single run from each subject. The benefits of the Bayesian GLM are quite apparent for single-run data, producing much smoother estimates of activation amplitude and much larger areas of activation at the individual level. The areas of activation in individual subjects, though somewhat smaller than those based on both runs, are already reflective of unique patterns of functional topology.

## 4.3 High group-level power in small samples

A unique feature of this spatial Bayesian GLM is its ability to be easily extended to group-level analysis in a computationally efficient way. Spatial Bayesian modeling is often assumed to be primarily beneficial for subject-level analysis, as the classical GLM tends to produce highly noisy estimates and under-powered areas of activation due to the low signal-to-noise ratio (SNR) in task fMRI data [Welvaert and Rosseel, 2013]. However, we also observe clear benefits of the Bayesian GLM for group-level analysis. Namely, we observe improved test-retest reliability of group-average estimates of activation amplitude and substantially increased power to detect activations. Notably, the power of the Bayesian GLM to detect activations above 0.5% signal change is remarkably consistent across sample sizes from  $n = 10$  to  $n = 45$ . This illustrates that the Bayesian GLM has high power to detect activations above a scientifically meaningful effect size even in small samples. The high power of the Bayesian GLM and the ability to explicitly consider effect size can help avoid the concerning issue of effect size dependence on sample size in the classical GLM [Geuter et al., 2018].

## 4.4 Efficient Bayesian computation

While the benefits of spatial Bayesian modeling for task fMRI analysis have been long recognized [Zhang et al., 2014, 2015, 2016, Guhaniyogi et al., 2017, Spencer et al., 2020], previous methods for volumetric fMRI were constrained by high computational demands. Analyzing cortical surface data has the dual benefit of leveraging scientifically relevant spatial dependencies along the cortical surface and of dramatically reducing dimensionality, facilitating efficient computation. The surface-based spatial Bayesian GLM also leverages recent advances in Bayesian computation and spatial statistics to maximize both computational efficiency and accuracy in model estimation. Areas of activation are based on the joint posterior distribution using an efficient Bayesian computation approach, which maximizes power to detect activations [Bolin and Lindgren, 2018].

It is important to note that the Bayesian GLM takes substantially more computation time, memory and processing requirements compared to a massive univariate approach. Indeed, such approaches were originally designed for maximal computational efficiency, given the much more limited computing power available in the early days of task fMRI. Today, statistical and computational advances make it quite feasible to use more sophisticated techniques to extract more accurate and nuanced information from task fMRI studies. In our analysis, model estimation per hemisphere requires approximately 1.5 hours for each individual subject and approximately 3 hours for group-level analysis with  $n = 45$ . While this certainly represents a greater investment of time than the classical GLM, it is a small fraction of the time and resources already invested in experimental design, participant recruitment, data collection, and data processing. Therefore, the benefits of the Bayesian GLM are likely worth the computational tradeoff.

## 4.5 Software implementation

The surface-based spatial Bayesian GLM is implemented in the R package **BayesfMRI**, which is designed to be maximally convenient from a user perspective. The main function in **BayesfMRI** can be used to directly analyze surface data in CIFTI and GIFTI format and performs all processing steps described in this paper, including resampling, scaling, nuisance regression and prewhitening using a high-order, spatially varying AR process. Integration with the **ciftiTools** R package [Pham and Mejia, 2021] allows for direct visualization of estimates and areas of activation in R, as well as the ability to write out results in CIFTI or GIFTI format.

## 4.6 Study limitations

This study is subject to several important limitations. First, here we analyze data from the young adult HCP, a large repository containing high-quality fMRI data acquired using multi-band techniques optimized for high cortical SNR. Our findings are therefore reflective of the HCP acquisition and processing and the study population. In other contexts, our findings would surely be somewhat different. However, given the quality of HCP data, particularly on the cortical surface, it represents something of a best-case scenario for the classical GLM. In higher-noise data, surface-based spatial Bayesian modeling may prove to be even more beneficial.

Second, our analyses are based on test-retest data in lieu of information on the ground truth of task activation at the individual and group level. Furthermore, for analyses using MSE and correlation, we utilize the *classical GLM* estimates of activation as a noisy but unbiased proxy for the ground truth to avoid bias in favor of the Bayesian GLM. Our measures of reliability are therefore also subject to noise. Although this results in an imperfect assessment of reliability, the consistency of our results across subjects, tasks and samples provides clear evidence of the benefits of the Bayesian GLM.

Finally, here we limit our analysis to the cortical surface, excluding subcortical and cerebellar regions. These areas represent great scientific interest and importance. Given the low SNR in the subcortex, particularly in HCP-style multiband data, spatial Bayesian modeling may be particularly beneficial for these regions. While the current implementation of the Bayesian GLM considered here is limited to the cortical surface, extension to subcortical and cerebellar regions is an important area for future research.

## 4.7 Future work

In ongoing and future work, we plan several extensions and improvements to the surface-based spatial Bayesian GLM. First, we are developing an alternative empirical Bayesian computation approach using expectation-

maximization (EM) for greater computational efficiency and flexibility. Second, we plan to extend the spatial Bayesian GLM to subcortical and cerebellar regions, which are also of interest in the neuroscience research community. Third, we plan on investigating the value of using the full-resolution cortical surface data in conjunction with a mesh that uses fewer points than data locations to see if there is an inferential benefit to using the full-resolution data over using data resampled to a computationally feasible resolution. Finally, we plan to directly integrate HRF derivatives into the Bayesian model to fully account for variability in the temporal properties of the hemodynamic response. These improvements and extensions will be incorporated into future versions of the **BayesfMRI** R package.

Future work should assess the *value* of the improvement in subject-level reliability of the Bayesian GLM. Does the improvement in reliability lead to better prediction of behavioral measures, such as task performance? Are the unique functional topologies that we see reflected in subject-level areas of activation reliable enough to serve as a “fingerprint”, whereby a subject is identifiable based on these patterns? Future work should also assess the effect of the Bayesian GLM on the scan duration necessary to produce highly reliable estimates and areas of activation. For example, how much data is required at the subject level to produce estimates that are predictive of behavior, or functional topologies that are identifiable? These questions are important to address in order to better understand the true benefits of surface-based spatial Bayesian modeling, in terms of extracting not only reliable but informative measures of task activation in individuals, and of reducing the burden of long and repeated scanning sessions to achieve these goals.

## 5 Conclusion

In this study, we assess the reliability of individual and group-average task activations produced by a surface-based spatial Bayesian general linear model (GLM), compared with the classical “massive univariate” GLM. Based on an analysis of test-retest motor task fMRI data from the Human Connectome Project, we find that surface-based spatial Bayesian modeling produces more reliable subject-level and group-average estimates of activation amplitude and highly consistent subject-level areas of activation. Furthermore, the Bayesian GLM has high power to detect activations in individuals and small group studies. The Bayesian GLM is computationally efficient at both the subject and group level and is conveniently implemented in the R package **BayesfMRI**. The ease of implementation makes this powerful method widely accessible.

The code used to perform the analyses and produce the visualizations used in this validation study can be found online via GitHub<sup>2</sup>.

## 6 Acknowledgments

Data collection and sharing for this project was provided by the MGH-USC Human Connectome Project (HCP; Principal Investigators: Bruce Rosen, M.D., Ph.D., Arthur W. Toga, Ph.D., Van J. Weeden, MD). HCP funding was provided by the National Institute of Dental and Craniofacial Research (NIDCR), the National Institute of Mental Health (NIMH), and the National Institute of Neurological Disorders and Stroke (NINDS). HCP data are disseminated by the Laboratory of Neuro Imaging at the University of Southern California.

The research of Daniel Spencer and Amanda Mejia is partially funded by the National Institute of Biomedical Imaging and Bioengineering (R01EB027119).

---

<sup>2</sup>[https://github.com/danieladamspencer/BayesGLM\\_Validation](https://github.com/danieladamspencer/BayesGLM_Validation)

## References

- Christie Alappat, Achim Basermann, Alan R. Bishop, Holger Fehske, Georg Hager, Olaf Schenk, Jonas Thies, and Gerhard Wellein. A recursive algebraic coloring technique for hardware-efficient symmetric sparse matrix-vector multiplication. *ACM Trans. Parallel Comput.*, 7(3), June 2020. ISSN 2329-4949. doi: 10.1145/3399732. URL <https://doi.org/10.1145/3399732>.
- Alan Anticevic, Donna L Dierker, Sarah K Gillespie, Grega Repovs, John G Csernansky, David C Van Essen, and Deanna M Barch. Comparing surface-based and volume-based analyses of functional neuroimaging data in patients with schizophrenia. *Neuroimage*, 41(3):835–848, 2008.
- Deanna M Barch, Gregory C Burgess, Michael P Harms, Steven E Petersen, Bradley L Schlaggar, Maurizio Corbetta, Matthew F Glasser, Sandra Curtiss, Sachin Dixit, Cindy Feldt, et al. Function in the human connectome: task-fMRI and individual differences in behavior. *Neuroimage*, 80:169–189, 2013.
- John J Bartko. The intraclass correlation coefficient as a measure of reliability. *Psychological reports*, 19(1):3–11, 1966.
- Yoav Benjamini and Yosef Hochberg. Controlling the false discovery rate: a practical and powerful approach to multiple testing. *Journal of the Royal Statistical Society: Series B (Methodological)*, 57(1):289–300, 1995.
- David Bolin and Finn Lindgren. A comparison between Markov approximations and other methods for large spatial data sets. *Computational Statistics & Data Analysis*, 61:7–21, 2013.
- David Bolin and Finn Lindgren. Excursion and contour uncertainty regions for latent Gaussian models. *Journal of the Royal Statistical Society: Series B: Statistical Methodology*, pages 85–106, 2015.
- David Bolin and Finn Lindgren. Calculating probabilistic excursion sets and related quantities using excursions. *Journal of Statistical Software*, 86(5):1–20, 2018. doi: 10.18637/jss.v086.i05.
- Matthias Bollhöfer, Aryan Eftekhari, Simon Scheidegger, and Olaf Schenk. Large-scale sparse inverse covariance matrix estimation. *SIAM Journal on Scientific Computing*, 41(1):A380–A401, 2019. doi: 10.1137/17M1147615. URL <https://doi.org/10.1137/17M1147615>.
- Matthias Bollhöfer, Olaf Schenk, Radim Janalik, Steve Hamm, and Kiran Gullapalli. *Parallel Algorithms in Computational Science and Engineering*. Springer International Publishing, Cham, 2020. ISBN 978-3-030-43736-7. doi: 10.1007/978-3-030-43736-7\_1. URL [https://doi.org/10.1007/978-3-030-43736-7\\_1](https://doi.org/10.1007/978-3-030-43736-7_1).
- Rodrigo M Braga and Randy L Buckner. Parallel interdigitated distributed networks within the individual estimated by intrinsic functional connectivity. *Neuron*, 95(2):457–471, 2017.
- Peter J Brockwell, Peter J Brockwell, Richard A Davis, and Richard A Davis. *Introduction to time series and forecasting*. Springer, 2016.
- Stefan Brodoehl, Christian Gaser, Robert Dahnke, Otto W Witte, and Carsten M Klingner. Surface-based analysis increases the specificity of cortical activation patterns and connectivity results. *Scientific reports*, 10(1):1–13, 2020.
- Danilo Bzdok and BT Thomas Yeo. Inference in the age of big data: Future perspectives on neuroscience. *Neuroimage*, 155:549–564, 2017.
- Ann S Choe, Craig K Jones, Suresh E Joel, John Muschelli, Visar Belegu, Brian S Caffo, Martin A Lindquist, Peter CM van Zijl, and James J Pekar. Reproducibility and temporal structure in weekly resting-state fMRI over a period of 3.5 years. *PloS one*, 10(10):e0140134, 2015.
- Domenic V Cicchetti. Guidelines, criteria, and rules of thumb for evaluating normed and standardized assessment instruments in psychology. *Psychological assessment*, 6(4):284, 1994.
- Henk R Cremers, Tor D Wager, and Tal Yarkoni. The relation between statistical power and inference in fmri. *PloS one*, 12(11):e0184923, 2017.
- Lee R Dice. Measures of the amount of ecologic association between species. *Ecology*, 26(3):297–302, 1945.
- Maxwell L Elliott, Annchen R Knodt, David Ireland, Meriwether L Morris, Richie Poulton, Sandhya Ramrakha, Maria L Sison, Terrie E Moffitt, Avshalom Caspi, and Ahmad R Hariri. What is the test-retest reliability of common task-functional MRI measures? new empirical evidence and a meta-analysis. *Psychological Science*, 31(7):792–806, 2020.

- Bruce Fischl. Freesurfer. *Neuroimage*, 62(2):774–781, 2012.
- Bruce Fischl, Martin I Sereno, and Anders M Dale. Cortical surface-based analysis: II: inflation, flattening, and a surface-based coordinate system. *Neuroimage*, 9(2):195–207, 1999.
- Karl J Friston, Andrew P Holmes, JB Poline, PJ Grasby, SCR Williams, Richard SJ Frackowiak, and Robert Turner. Analysis of fMRI time-series revisited. *Neuroimage*, 2(1):45–53, 1995.
- Karl J Friston, P Fletcher, Oliver Josephs, ANDREW Holmes, MD Rugg, and Robert Turner. Event-related fMRI: characterizing differential responses. *Neuroimage*, 7(1):30–40, 1998.
- Stephan Geuter, Guanghao Qi, Robert C Welsh, Tor D Wager, and Martin A Lindquist. Effect size and power in fmri group analysis. *Biorxiv*, page 295048, 2018.
- Matthew F Glasser, Stamatios N Sotiropoulos, J Anthony Wilson, Timothy S Coalson, Bruce Fischl, Jesper L Andersson, Junqian Xu, Saad Jbabdi, Matthew Webster, Jonathan R Polimeni, et al. The minimal preprocessing pipelines for the Human Connectome Project. *Neuroimage*, 80:105–124, 2013.
- Gary H Glover. Deconvolution of impulse response in event-related BOLD fMRI. *Neuroimage*, 9(4):416–429, 1999.
- Evan M. Gordon, Timothy O. Laumann, Adrian W. Gilmore, Dillan J. Newbold, Deanna J. Greene, Jeffrey J. Berg, Mario Ortega, Catherine Hoyt-Drazen, Caterina Gratton, Haoxin Sun, Jacqueline M. Hampton, Rebecca S. Coalson, Annie Nguyen, Kathleen B. McDermott, Joshua S. Shimony, Abraham Z. Snyder, Bradley L. Schlaggar, Steven E. Petersen, Steven M. Nelson, and Nico U.F. Dosenbach. "The Midnight Scan Club (MSC) dataset", 2020.
- Rajarshi Guhaniyogi, Shaan Qamar, and David B Dunson. Bayesian tensor regression. *The Journal of Machine Learning Research*, 18(1):2733–2763, 2017.
- Ru Kong, Jingwei Li, Csaba Orban, Mert R Sabuncu, Hesheng Liu, Alexander Schaefer, Nanbo Sun, Xi-Nian Zuo, Avram J Holmes, Simon B Eickhoff, et al. Spatial topography of individual-specific cortical networks predicts human cognition, personality, and emotion. *Cerebral cortex*, 29(6):2533–2551, 2019.
- Timothy O Laumann, Evan M Gordon, Babatunde Adeyemo, Abraham Z Snyder, Sung Jun Joo, Mei-Yen Chen, Adrian W Gilmore, Kathleen B McDermott, Steven M Nelson, Nico UF Dosenbach, Bradley L Schlaggar, Jeanette A Mumford, Russell A Poldrack, and Steven E Petersen. Functional system and areal organization of a highly sampled individual human brain. *Neuron*, 87(3):657–670, 2015.
- Finn Lindgren and Håvard Rue. Bayesian spatial modelling with R-INLA. *Journal of Statistical Software*, 63(19):1–25, 2015. URL <http://www.jstatsoft.org/v63/i19/>.
- Finn Lindgren, Håvard Rue, and Johan Lindström. An explicit link between Gaussian fields and Gaussian Markov random fields: the stochastic partial differential equation approach. *Journal of the Royal Statistical Society: Series B (Statistical Methodology)*, 73(4):423–498, 2011.
- Martin A Lindquist and Amanda Mejia. Zen and the art of multiple comparisons. *Psychosomatic medicine*, 77(2):114, 2015.
- Amanda F Mejia, Mary Beth Nebel, Yikai Wang, Brian S Caffo, and Ying Guo. Template independent component analysis: Targeted and reliable estimation of subject-level brain networks using big data population priors. *Journal of the American Statistical Association*, 115(531):1151–1177, 2020a.
- Amanda F Mejia, Yu Yue, David Bolin, Finn Lindgren, and Martin A Lindquist. A Bayesian general linear modeling approach to cortical surface fMRI data analysis. *Journal of the American Statistical Association*, 115(530):501–520, 2020b.
- Michal Mikl, Radek Mareček, Petr Hlušík, Martina Pavlicová, Aleš Drastich, Pavel Chlebus, Milan Brázdil, and Petr Krupa. Effects of spatial smoothing on fmri group inferences. *Magnetic resonance imaging*, 26(4):490–503, 2008.
- Damon Pham and Amanda F Mejia. *ciftiTools: Tools for Reading and Visualizing CIFTI Brain Files*, 2021. URL <https://CRAN.R-project.org/package=ciftiTools>. R package version 0.2.2.
- Jean-Baptiste Poline, Keith J Worsley, Alan C Evans, and Karl J Friston. Combining spatial extent and peak intensity to test for activations in functional imaging. *Neuroimage*, 5(2):83–96, 1997.

- Håvard Rue, Sara Martino, and Nicolas Chopin. Approximate bayesian inference for latent gaussian models by using integrated nested laplace approximations. *Journal of the Royal Statistical Society: Series B (Methodological)*, 71(2):319–392, 2009.
- H Shou, A Eloyan, S Lee, Vadim Zipunnikov, AN Crainiceanu, MB Nebel, B Caffo, MA Lindquist, and Ciprian M Crainiceanu. Quantifying the reliability of image replication studies: the image intraclass correlation coefficient (I2C2). *Cognitive, Affective, & Behavioral Neuroscience*, 13(4):714–724, 2013.
- Per Siden, Anders Eklund, David Bolin, and Mattias Villani. Fast Bayesian whole-brain fMRI analysis with spatial 3D priors. *NeuroImage*, 146:211–225, 2017.
- Stephen M Smith and Thomas E Nichols. Threshold-free cluster enhancement: addressing problems of smoothing, threshold dependence and localisation in cluster inference. *Neuroimage*, 44(1):83–98, 2009.
- Daniel Spencer, Rajarshi Guhaniyogi, and Raquel Prado. Joint Bayesian estimation of voxel activation and inter-regional connectivity in fMRI experiments. *Psychometrika*, pages 1–25, 2020.
- Alan Tucholka, Virgile Fritsch, Jean-Baptiste Poline, and Bertrand Thirion. An empirical comparison of surface-based and volume-based group studies in neuroimaging. *Neuroimage*, 63(3):1443–1453, 2012.
- David C Van Essen, Stephen M Smith, Deanna M Barch, Timothy EJ Behrens, Essa Yacoub, Kamil Ugurbil, Wu-Minn HCP Consortium, et al. The wu-minn human connectome project: an overview. *Neuroimage*, 80: 62–79, 2013.
- Marijke Welvaert and Yves Rosseel. On the definition of signal-to-noise ratio and contrast-to-noise ratio for fmri data. *PLoS one*, 8(11):e77089, 2013.
- Linlin Zhang, Michele Guindani, Francesco Versace, and Marina Vannucci. A spatio-temporal nonparametric Bayesian variable selection model of fMRI data for clustering correlated time courses. *NeuroImage*, 95:162–175, 2014.
- Linlin Zhang, Michele Guindani, and Marina Vannucci. Bayesian models for functional magnetic resonance imaging data analysis. *Wiley Interdisciplinary Reviews: Computational Statistics*, 7(1):21–41, 2015.
- Linlin Zhang, Michele Guindani, Francesco Versace, Jeffrey M Engelmann, Marina Vannucci, et al. A spatiotemporal nonparametric Bayesian model of multi-subject fMRI data. *Annals of Applied Statistics*, 10(2):638–666, 2016.



## A Midthickness versus spherical surface distances

One of the advantages to using an SPDE prior is improved accounting for spatial dependence through subject-specific cortical surfaces. This offers an improvement by reducing the distance distortion resulting from using spherical surfaces (see figure A.1 in the Appendix). A comparison of the subject test-retest correlation using the spherical and midthickness surfaces can be seen in appendix figure C.4. The differences in the correlation between the models fit using the midthickness surfaces and spherical surfaces are small, but there is a small visible improvement in the median correlations in each task.

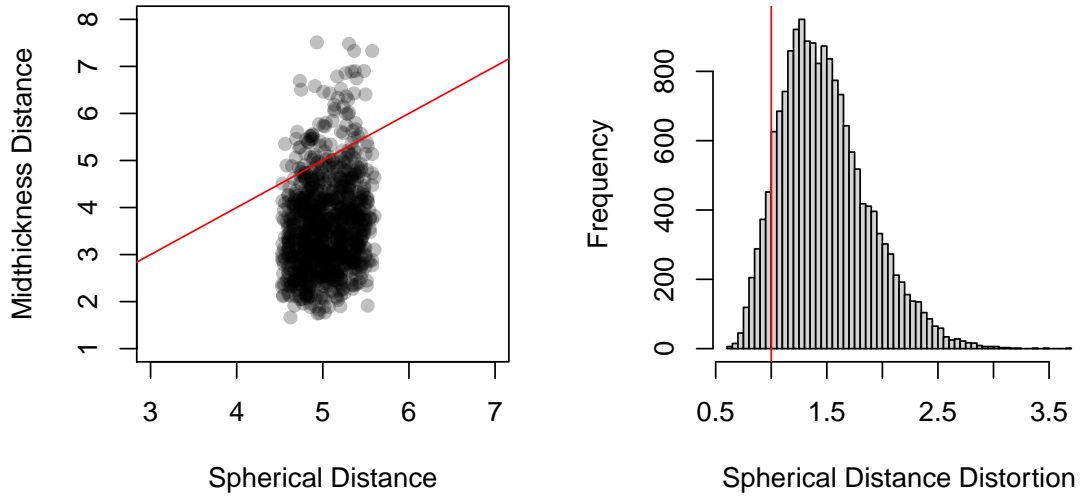
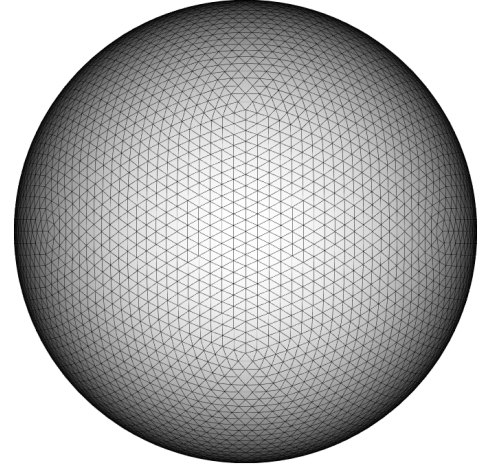


**Figure A.1: Distance distortions between neighboring vertices on spherical surface relative to midthickness surface.** For this analysis, group-average spherical and midthickness 32k surfaces were resampled to 6k using the Connectome Workbench. The distance between each pair of neighbors in the triangular mesh was computed for each surface. On the left-hand plot, a random sample of 1000 neighbors is shown. The red line indicates equality. Distances on the spherical surface are much more uniform and tend to be larger than those on the midthickness surface. The right panel shows the distribution of spherical distance distortions. The red line indicates no distortion. For each pair of neighboring vertices, spherical distance distortion is defined as the ratio of their distance on the spherical surface to their distance on the midthickness surface. Distortions range from approximately 0.5 (distance is halved on the spherical surface) to 3.5 (distance is over 3 times as large on the spherical surface).



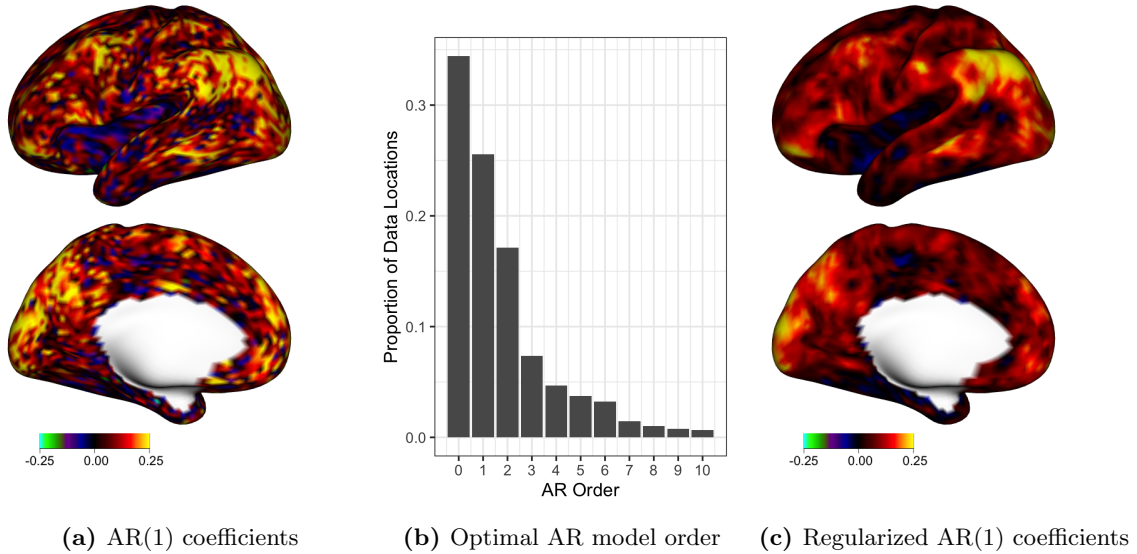
(a) Midthickness Surface (5k vertices)



(b) Spherical Surface (5k vertices)

**Figure A.2:** An example of the triangular mesh structure on the midthickness and spherical surface resampled to a resolution of around 5,000 vertices.

## B Prewhitening



(a) AR(1) coefficients

(b) Optimal AR model order

(c) Regularized AR(1) coefficients

**Figure B.3: Illustration of prewhitening procedure.** (a) Left hemisphere AR(1) coefficient estimates from a single subject and run. Systematic spatial variation in the degree of autocorrelation is clearly apparent. (b) Histogram of the optimal AR model order at each vertex, based on AIC. A low-order AR process (e.g. AR(1) or AR(2)) would fail to fully capture and remove the residual autocorrelation at many locations in the brain. (c) Left hemisphere estimates of the AR(1) coefficient at each vertex after regularization through averaging over runs and surface smoothing at 5mm FWHM.

## C Robustness of the resampled classical GLM

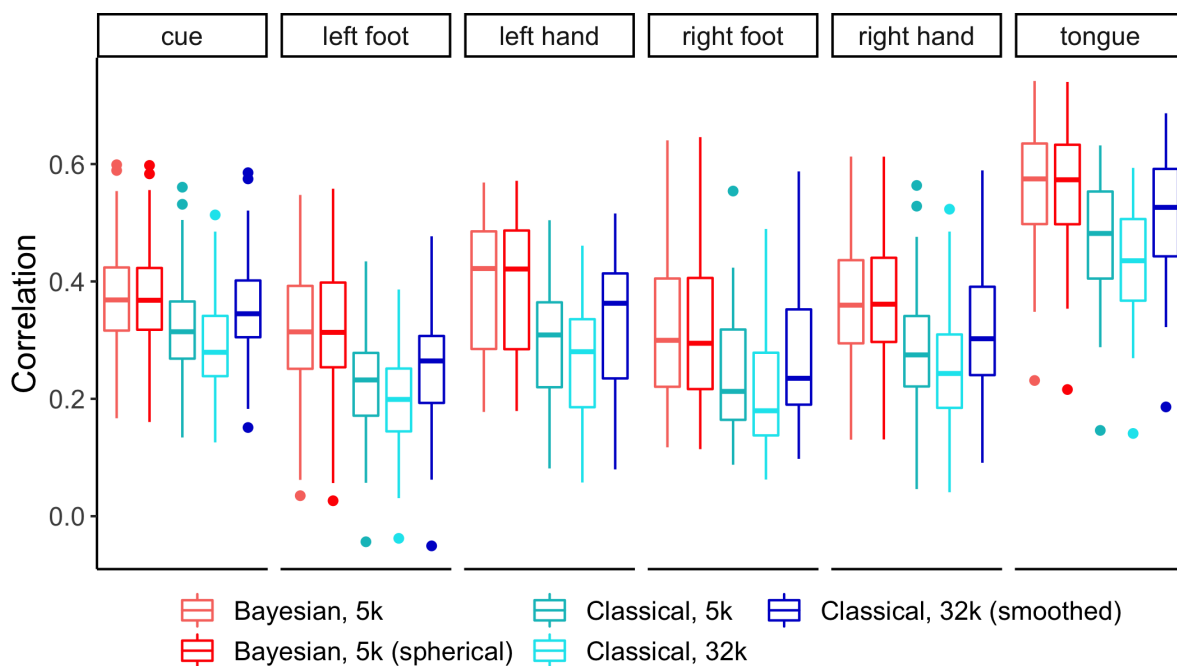


**Figure C.4:** Subject-level test-retest correlation for the SBSB GLM and classical GLM performed on 5k-resolution data and the classical GLM performed on full-resolution data (32k) with unsmoothed and smoothed data. The performance of the SBSB GLM using spherical surfaces is also shown.

## D Additional reliability analysis figures

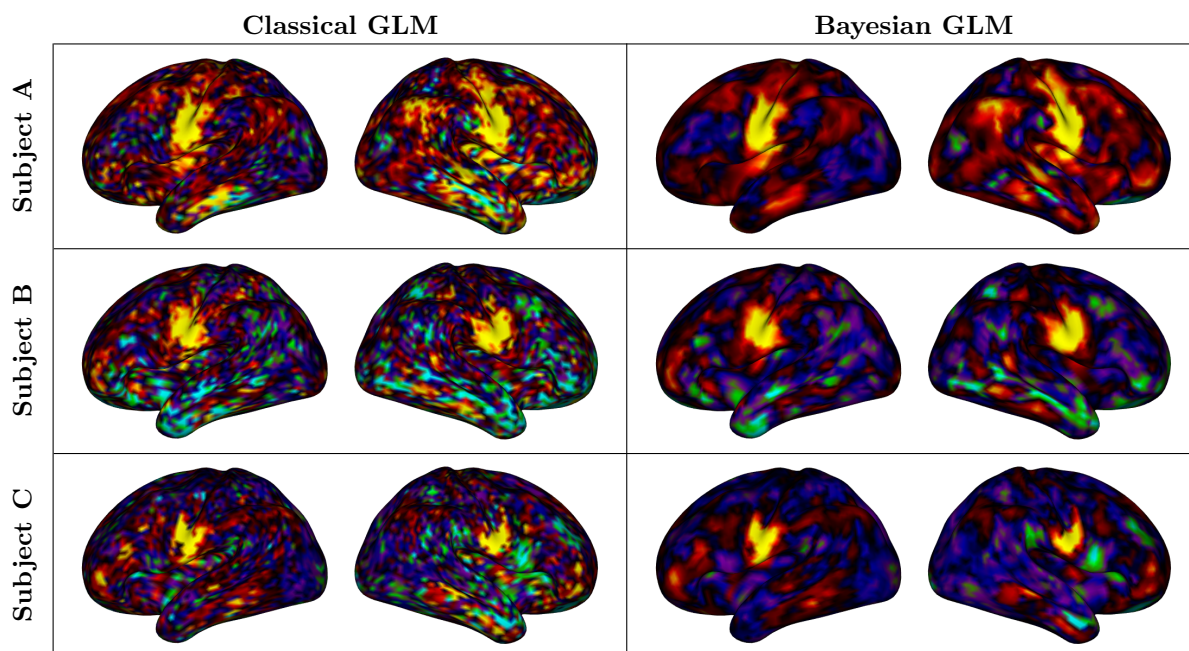


**Figure D.5:** Single run (LR) amplitude estimation results for subjects A, B, and C.

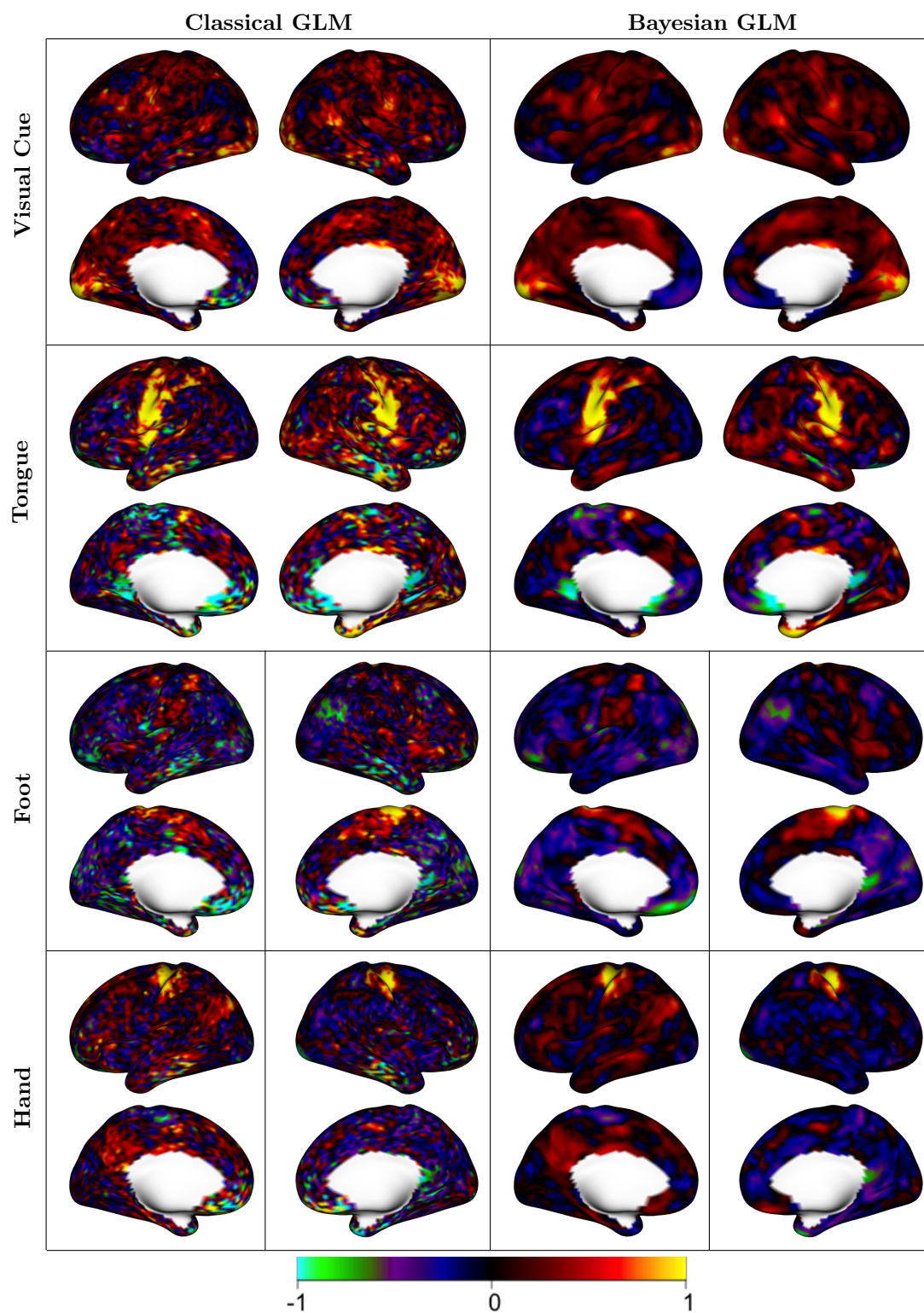


**Figure D.6:** Subject-level estimates of activation for each motor task and the visual cue, in units of local percent signal change. For lateral tasks, only the contralateral hemisphere is displayed. Using the surface-based spatial Bayesian GLM, estimates of activation are smoother, and individual topology of activation is more apparent.



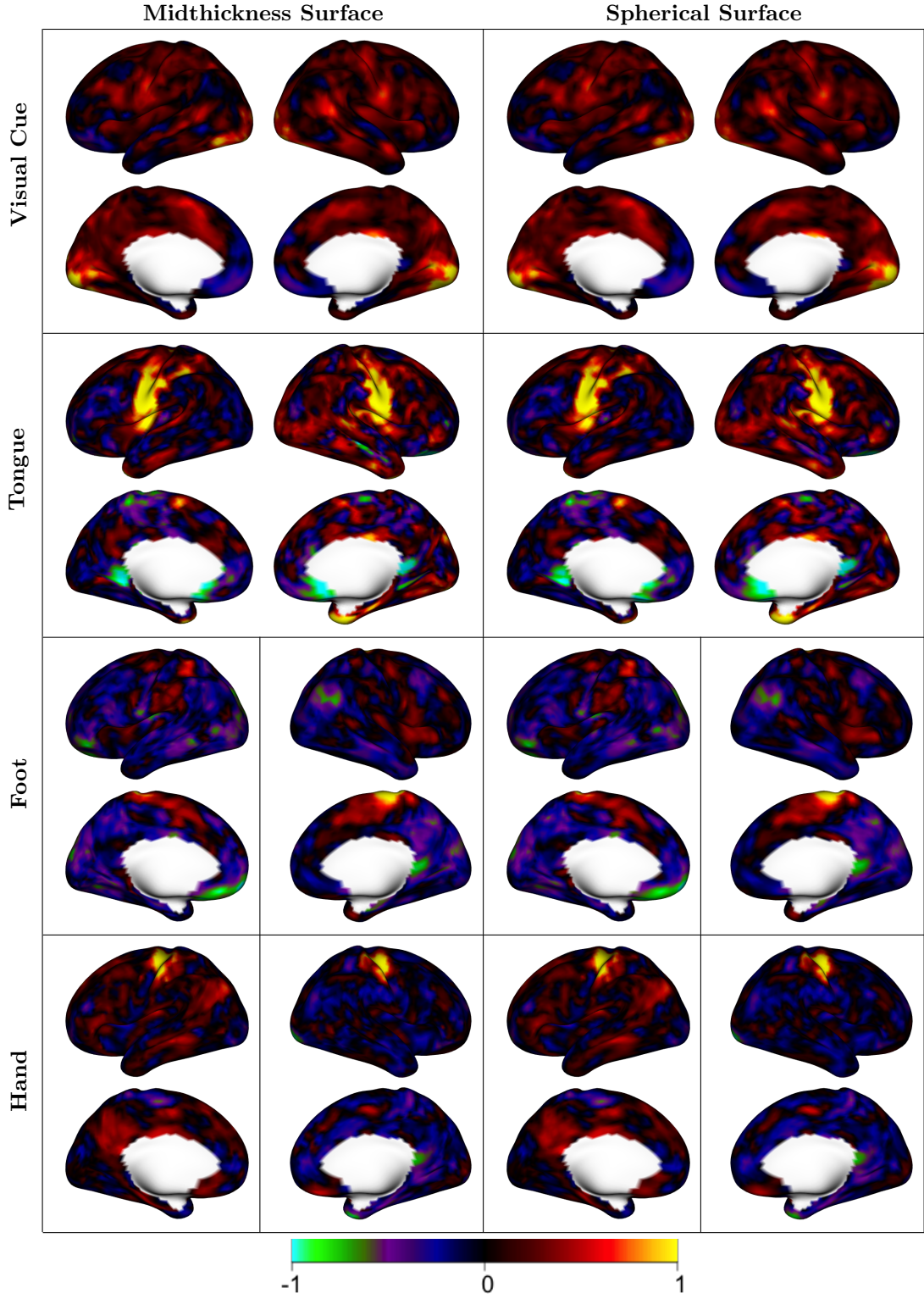


**Figure D.7:** Subject-level Bayesian estimates of activation amplitude for each motor task and the visual cue, in units of local percent signal change. For lateral tasks, only the contralateral hemisphere is displayed. Though the analyses were completed using different surfaces on the same data, the results here are shown using the inflated midthickness surface in order to make a direct comparison between the use of the two surfaces. Analysis done using the subject-specific midthickness surfaces shows better localization to the motor cortex for the hand and foot tasks.

To provide a single measure of reliability for each image of activation, we use a weighted version of the image intraclass correlation coefficient (I2C2) [Shou et al., 2013], calculated as

$$\text{wICC} = \frac{\sum_v \lambda_v \sigma_{b,v}^2}{\sum_v \lambda_v \sigma_{t,v}^2},$$

where the weights  $\lambda_v$  on each vertex are incorporated to more strongly weight certain areas of the image. Here, we use the classical GLM estimates of group-level activation as the basis for the weights. This reflects the relative importance of areas that are known to activate in the population, relative to areas that show little to no activation in the population. We adopt the weighted I2C2 in order to avoid giving credit to the Bayesian GLM simply for smoothing areas of little activation.

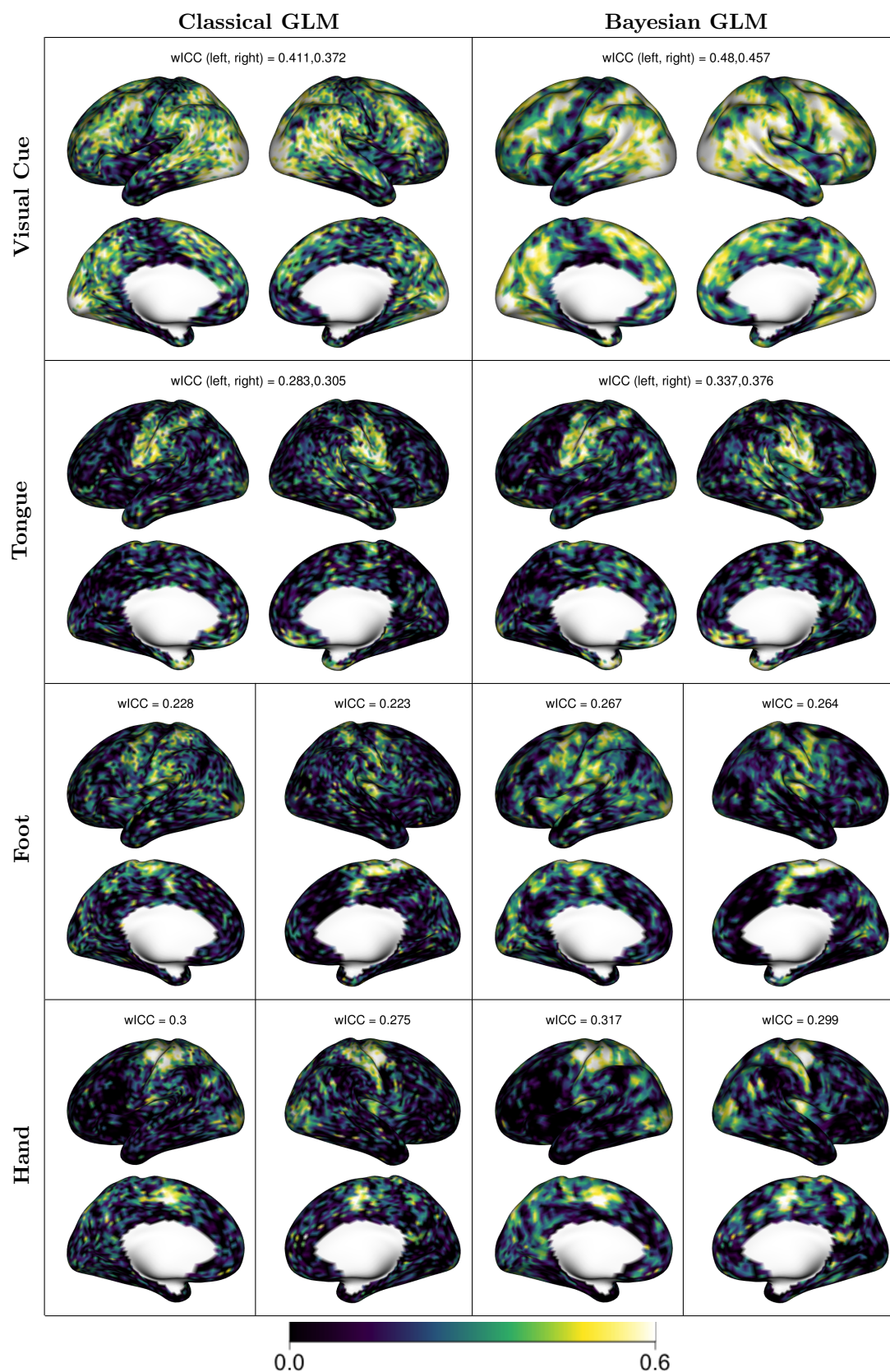


**Figure D.8:** The intraclass correlation coefficient (ICC) values across the six motor tasks.

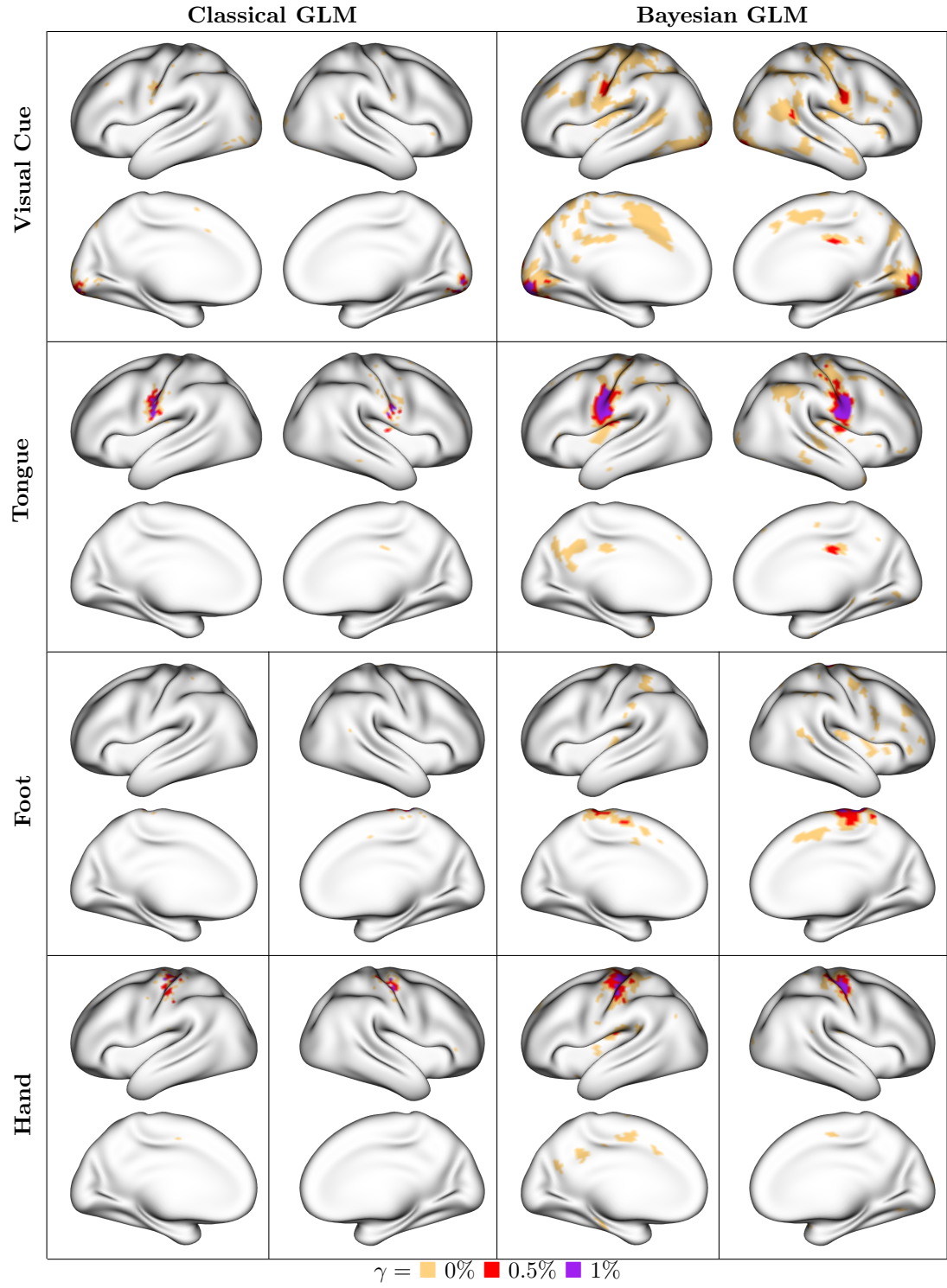


**Figure D.9:** Single-run activation maps for one subject across all six tasks.



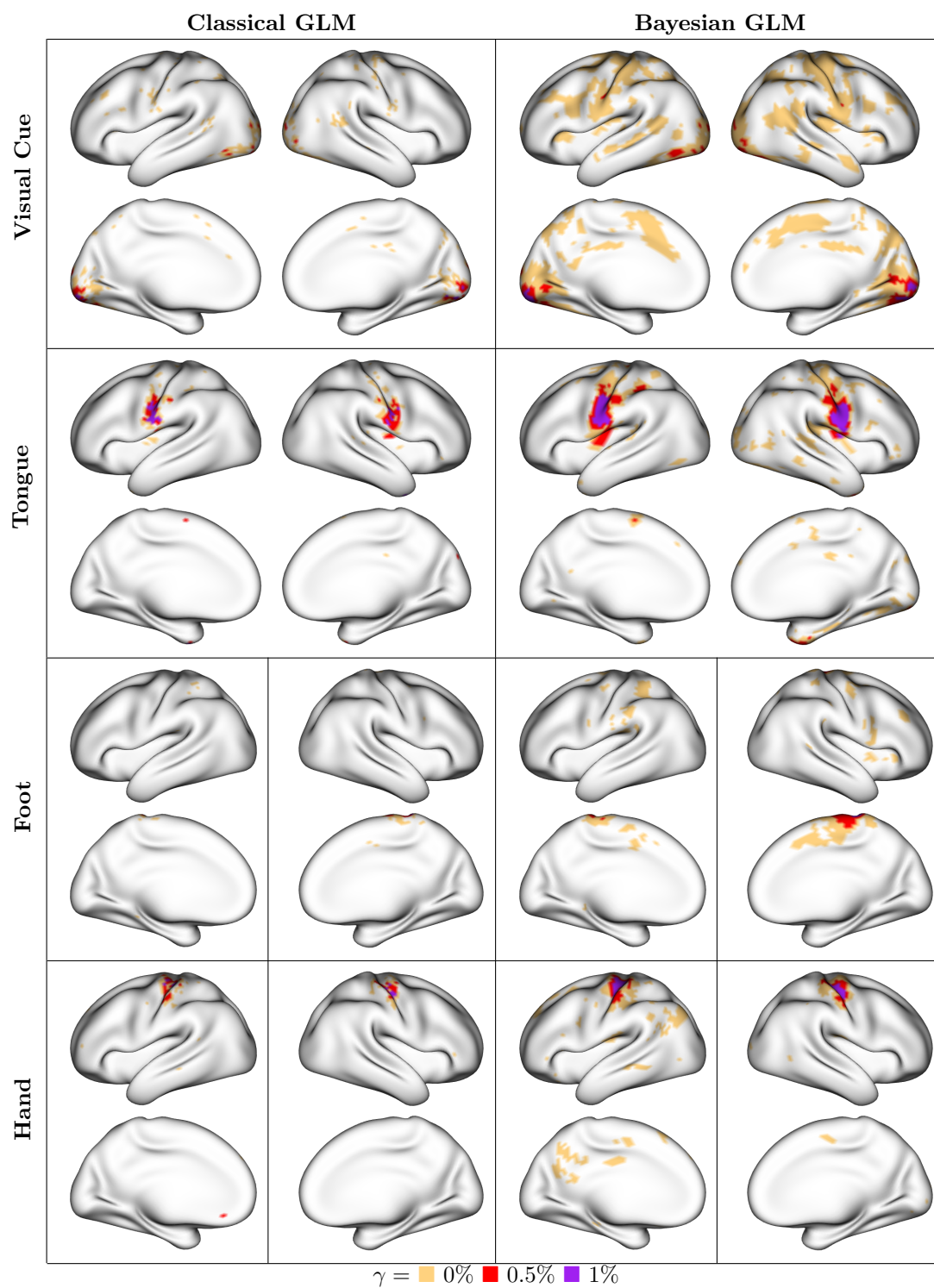


**Figure D.10:** Single-visit (two runs) activation maps for one subject across all six tasks.

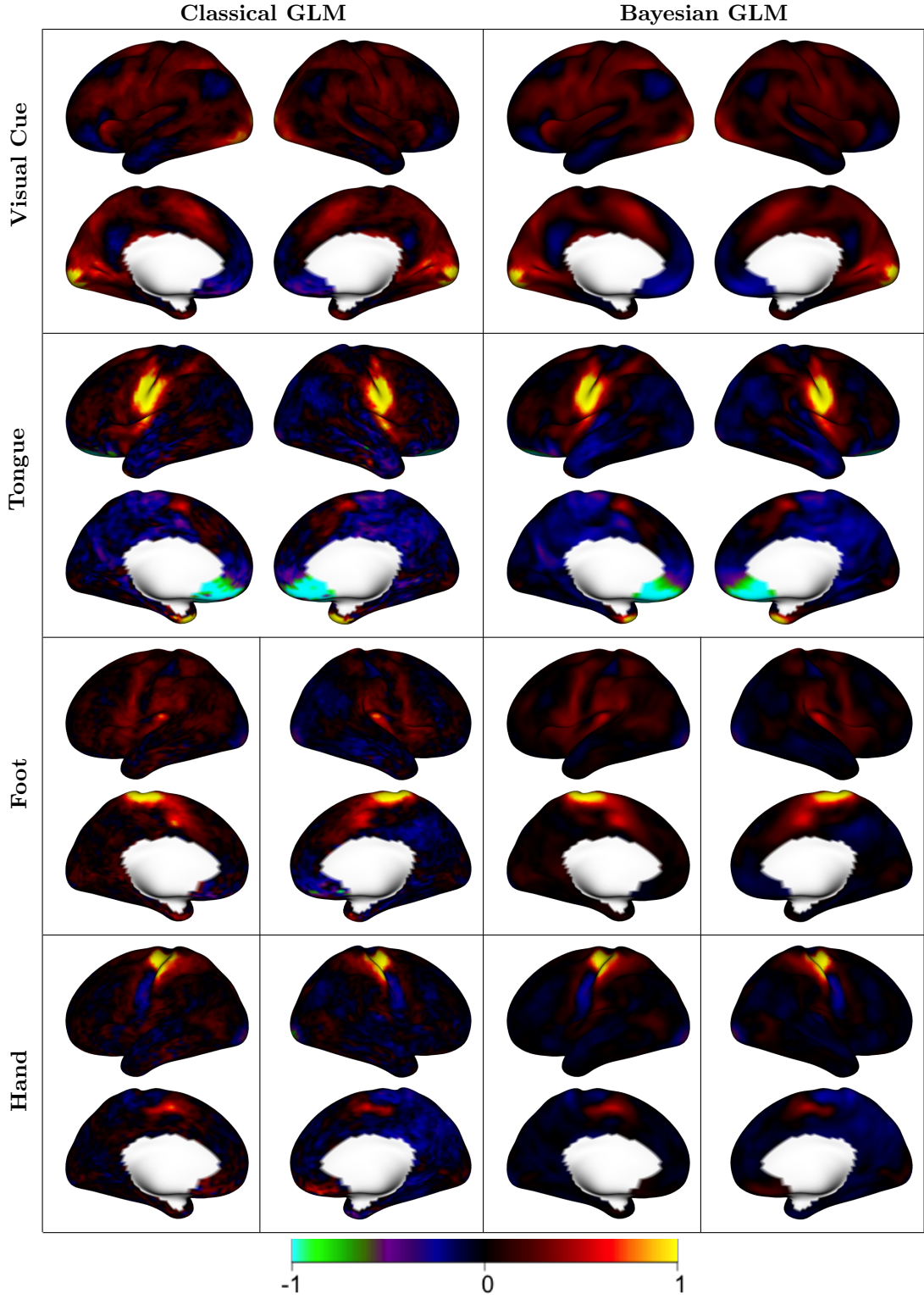


**Figure D.11:** Group-level estimates of activation for each motor task and the visual cue, in units of local percent signal change, based on the average across all subjects using the test data. For lateral tasks, only the contralateral hemisphere is displayed. Using the surface-based spatial Bayesian GLM, estimates of activation are smoother, even at the group level.

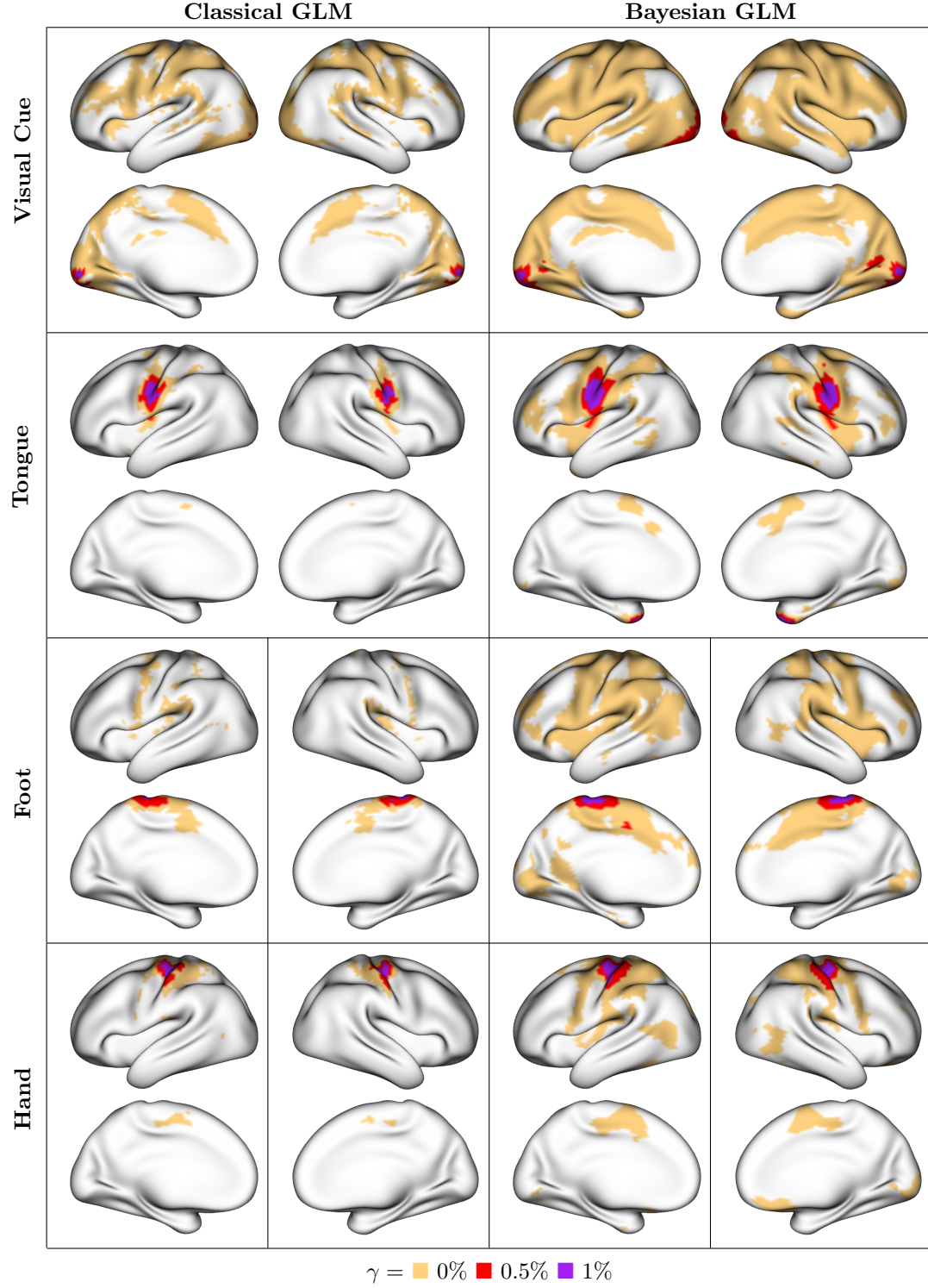


**Figure D.12:** Group-level activations found for each motor task and the visual cue for three different thresholds in percent signal change, based on the average across all subjects using the test data. For lateral tasks, only the contralateral hemisphere is displayed. Using the surface-based spatial Bayesian GLM, areas of activation are generally larger, especially at higher, more meaningful threshold levels such as  $\gamma = 0\%$  and  $\gamma = 0.5\%$ .